AD_____

AWARD NUMBER: W81XWH-08-1-0732

TITLE: High Resolution Diffusion Tensor Imaging of Cortical-Subcortical White Matter Tracts in TBI

PRINCIPAL INVESTIGATOR: Deborah M. Little, Ph.D.

CONTRACTING ORGANIZATION: University of Illinois, Chicago
Chicago, IL 60612

REPORT DATE: October 2009

TYPE OF REPORT: Annual

PREPARED FOR: U.S. Army Medical Research and Materiel Command
Fort Detrick, Maryland 21702-5012

REPORT DOCUMENTATION PAGE

Form Approved
OMB No. 0704-0188

1. REPORT DATE	2. REPORT TYPE	3. DATES COVERED
1 October 2009	Annual	15 Sep 2008 – 14 Sep 2009

4. TITLE AND SUBTITLE

High Resolution Diffusion Tensor Imaging of Cortical-Subcortical White Matter Tracts in TBI

5a. CONTRACT NUMBER

5b. GRANT NUMBER
W81XWH-08-1-0732

5c. PROGRAM ELEMENT NUMBER

6. AUTHOR(S)

Deborah M. Little, Ph.D.

E-Mail: little@uic.edu

5d. PROJECT NUMBER

5e. TASK NUMBER

5f. WORK UNIT NUMBER

7. PERFORMING ORGANIZATION NAME(S) AND ADDRESS(ES)

University of Illinois, Chicago
Chicago, IL 60612

8. PERFORMING ORGANIZATION REPORT NUMBER

9. SPONSORING / MONITORING AGENCY NAME(S) AND ADDRESS(ES)
U.S. Army Medical Research and Materiel Command
Fort Detrick, Maryland 21702-5012

10. SPONSOR/MONITOR'S ACRONYM(S)

11. SPONSOR/MONITOR'S REPORT NUMBER(S)

12. DISTRIBUTION / AVAILABILITY STATEMENT
Approved for Public Release; Distribution Unlimited

13. SUPPLEMENTARY NOTES

14. ABSTRACT
The most significant finding to date is the identification of what potentially may prove to be a central mechanism of cognitive impairment following traumatic brain injury. Although data collection is on-going as is data analysis, we focused in year 1 on validating and implementing analysis of integrity of thalamic projection fibers in a subgroup of 12 controls and 24 patients with TBI. The data show that cortical damage, long thought to be the underlying mechanism of impairment, does not account for cognitive impairment. Instead, our data demonstrate a strong relationship between thalamic projection fibers and executive function. A version of the manuscript is included. The data has been presented at the military research health conference, society for neurotrauma, and will be presented at the upcoming society for neuroscience. The manuscript received positive reviews at the first submission to Neurology and a revision is presently undergoing peer review at that journal.

15. SUBJECT TERMS
Traumatic brain injury, diffusion tensor imaging, executive function

16. SECURITY CLASSIFICATION OF:			17. LIMITATION OF ABSTRACT	18. NUMBER OF PAGES	19a. NAME OF RESPONSIBLE PERSON
a. REPORT	b. ABSTRACT	c. THIS PAGE			USAMRMC
U	U	U	UU	44	19b. TELEPHONE NUMBER *(include area code)*

Table of Contents

Introduction

The ***overall objective*** of the proposed research is to validate high resolution diffusion tensor imaging (DTI) as a diagnostic tool that would allow better characterization of patients who have sustained a mild to moderate closed head type TBI. The ***general hypothesis*** guiding this work is that TBI results in sustained changes in the white matter microstructure that can be assessed using DTI and that it is this change in white matter that results in chronic deficits in cognition. Our specific aims are to characterize: (i) and quantify neuropathology in frontal, temporal, and basal ganglia regions in chronic TBI using both diffusion tensor imaging and structural magnetic resonance imaging; (ii) white matter integrity of the cortical-subcortical fibers connecting basal ganglia and frontal regions using fiber tractography; (iii) the role of short-range (cortical u-fibers), as compared to long-range WM fiber tract integrity in TBI; (iv) cognitive function in chronic TBI using a neuropsychological test battery focused on executive function and attention. In order to accomplish the proposed aims, we will recruit 25 healthy controls and 50 TBI patients with closed head injuries ranging from mild to moderate in injury severity who are a minimum of 6 months post injury. In addition to MRI and DTI imaging these patients will also undergo neuropsychological testing with a focus on executive function and attention tasks.

Body

In the funded grant, we proposed to accomplish a number of concrete tasks in Year 1. These include (1) Completing all required administrative approvals and university approvals for the initiation of new research, (2) obtaining human subjects approvals through the Army, (3) begin subject recruitment which will continue throughout the life of the grant, (4) hire a research assistant to help accomplish these aims, (5) finalize the imaging protocol and complete quality assurance testing, (6) recruit and test 25 subjects, (7) begin work on analysis protocols using these first 25 subjects, (8) carry out quality assurance testing on all data that has been acquired. All of these items have been completed. We provide specific details below.

All university approvals were obtained in the first quarter of the grant. Human subjects approvals were obtained on 06-16-08. The annual continuing review, which included no protocol deviations or adverse events, was approved via convened review on 06-23-09. Continuing approval through the Army was granted on 08-06-09 (A-15142).

A research assistant (Michelle Siroko) was hired on 10-01-08. She is still employed and working on this grant.

The first 6 months of the grant included the analysis of pilot data to ensure an appropriate imaging protocol, validation of that protocol, and initiation of that imaging protocol. All training of the RA was conducted during this period including supervised validation of the neuropsychological protocol. In terms of human subjects data collection, a total of 27 subjects have completed the protocol to date. We describe the analyses that we have conducted on these 27 subjects below. We have also collected quality assurance data 14 times during the past year. This data is also presented below. There was a period of time of poor scanner quality identified via our quality assurance testing. This was identified and, in collaboration with GE, was fixed during the second quarter of the grant.

Quality Assurance Data

Monthly, a phantom data set using the same pulse sequences as for the human data, are collected. The imaging parameters for this quality assurance protocol are: TR/TE=5000/64ms, b=0,1000 s/mm^2, diffusion directions=27, FOV=20x20cm^2, matrix=256x256, slice thickness/gap=3/0mm, slices=7, NEX=8, and acceleration factor=2.

In terms of signal stability, with the exception of the period noted above, the scanner has been consistent mean signal intensities ranging from 9900 to 10100. Error in signal has also been stable over time. This data is presented in Figure 1 Below.

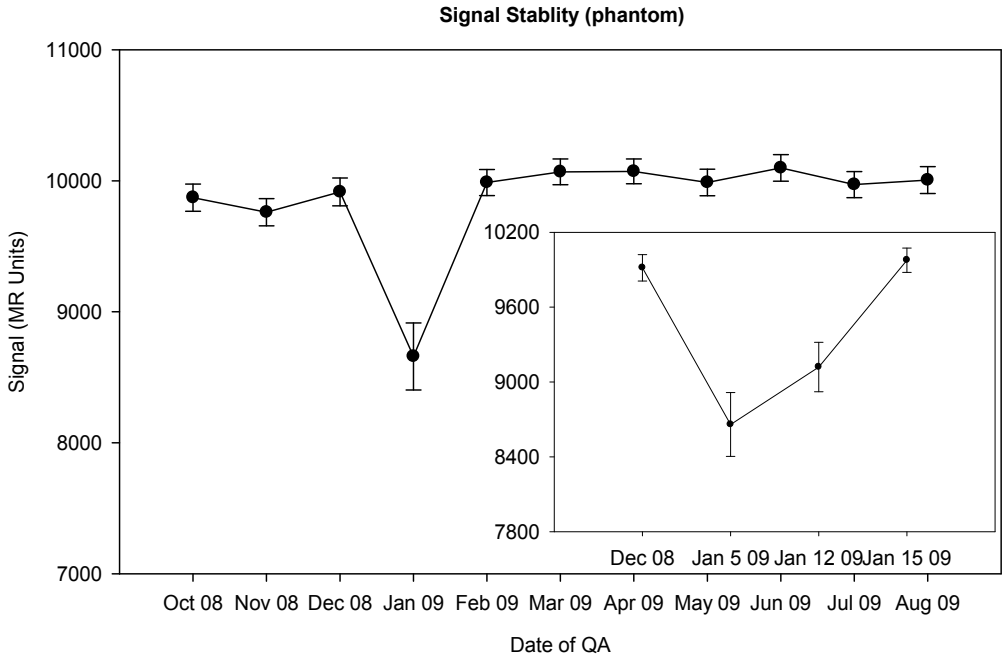

Figure 1. Scanner signal stability over year 1 of the grant via phantom testing.

It becomes obvious that the January QA testing identified a significant reduction in mean signal and increased variability over time. This is mirrored by assessments of increased noise presented below in Figure 2. The insert in Figure 1 shows follow up quality assurance testing conducted after GE site visits. Two visits were required to regain the signal that had been observed in December. As additional quality assurance testing was not budgeted, these additional interim QA tests was paid for by funds to the PI from the UIC college of medicine.

Scanner noise is assessed by placing a region of interest immediately lateral to the phantom. This provides a measure of background noise. With the exception of the period noted above noise as also been stable over time.

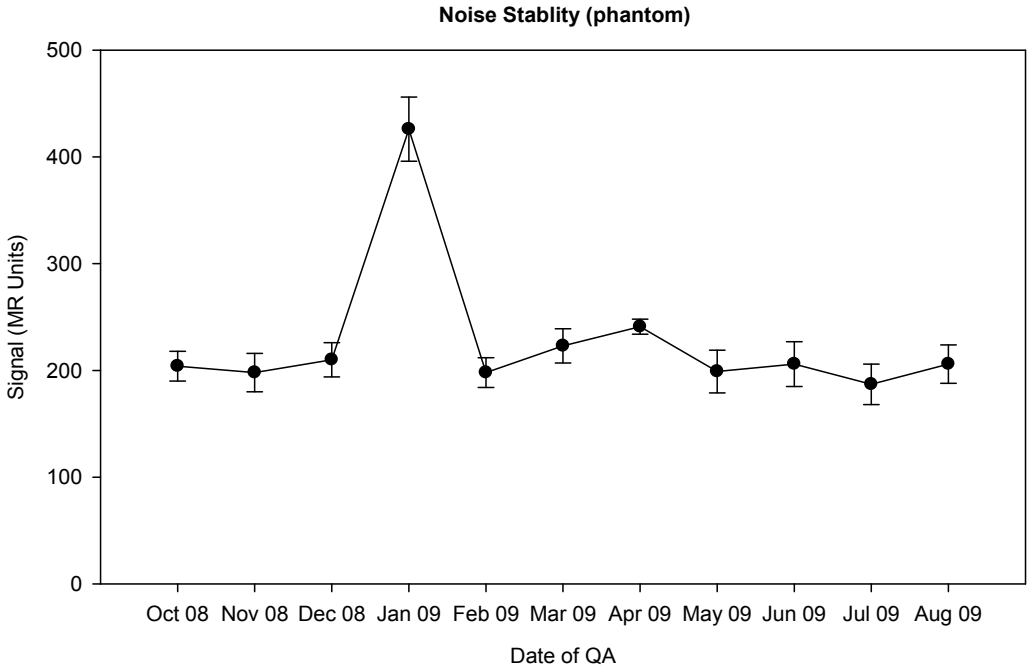

Figure 2. Scanner noise stability over year 1 of the grant via phantom testing.

Data from human subjects is assessed for each dataset. For human subjects noise and signal cannot be assessed in the same manner as our quality assurance data. As such, we use two indices. The first is peak to peak head motion as increased head motion will make the data unusable. Our threshold is 1 voxel of motion for a dataset to be included. In this study, the maximum motion allowable is 0.91 mm of in-plane movement. We present below in Figure 3, peak to peak head motion for each subject collected thus far. As can be seen in Figure 3, Subject 19 exceeds this threshold. Subject 27 would be considered borderline for inclusion.

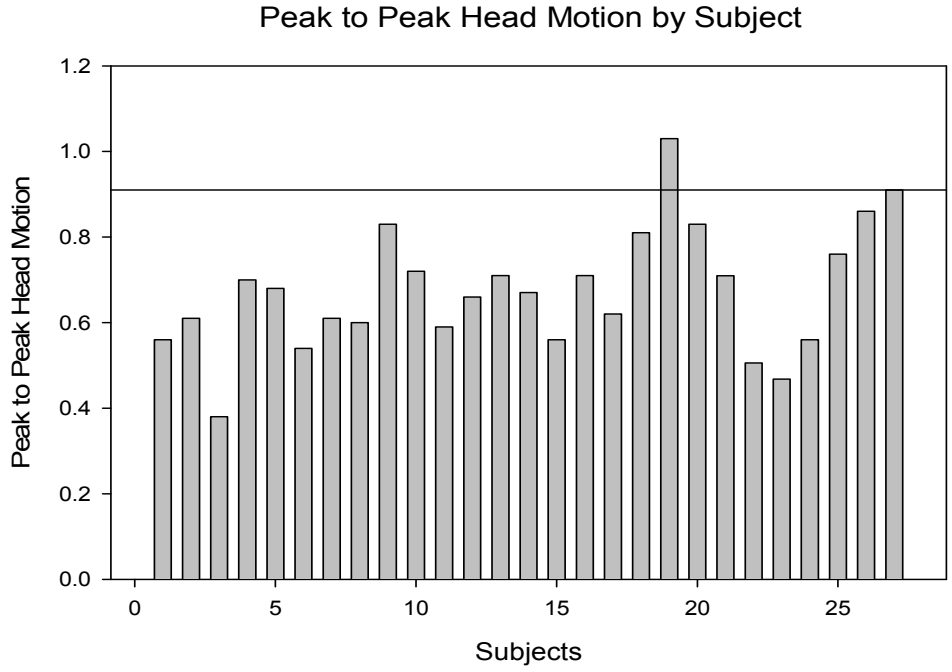

Figure 3. Head motion for each subject tested thus far.

Experimental Data Analysis Conducted to Date

During year 1 we have developed and validated methods for assessment of integrity of thalamic projection fibers. Details of the analysis, inter-rater reliability, and data is presented in Appendix 1 which is a manuscript presenting undergoing peer review (Revision 1) at Neurology.

Investigations of Thalamic Integrity in TBI

Briefly, we quantified the effects of traumatic brain injury on integrity of thalamo-cortical projection fibers and evaluated whether damage to these fibers accounts for impairments in executive function in chronic traumatic brain injury. To do this, we used high-resolution diffusion tensor magnetic resonance imaging of the thalamus on 24 patients with a history of single, closed-head traumatic brain injury (12 each of mild TBI and moderate to severe TBI) and 12 age- and education- matched controls. Detailed neuropsychological testing with an emphasis on executive function was also conducted. Fractional anisotropy was extracted from 12 regions of interest in cortical and corpus callosum structures and 7 subcortical regions of interest (anterior, ventral anterior, ventral lateral, dorsomedial, ventral posterior lateral, ventral posterior medial and pulvinar thalamic nuclei). The methods used to identify these nuclei are presented in Figure 4 below.

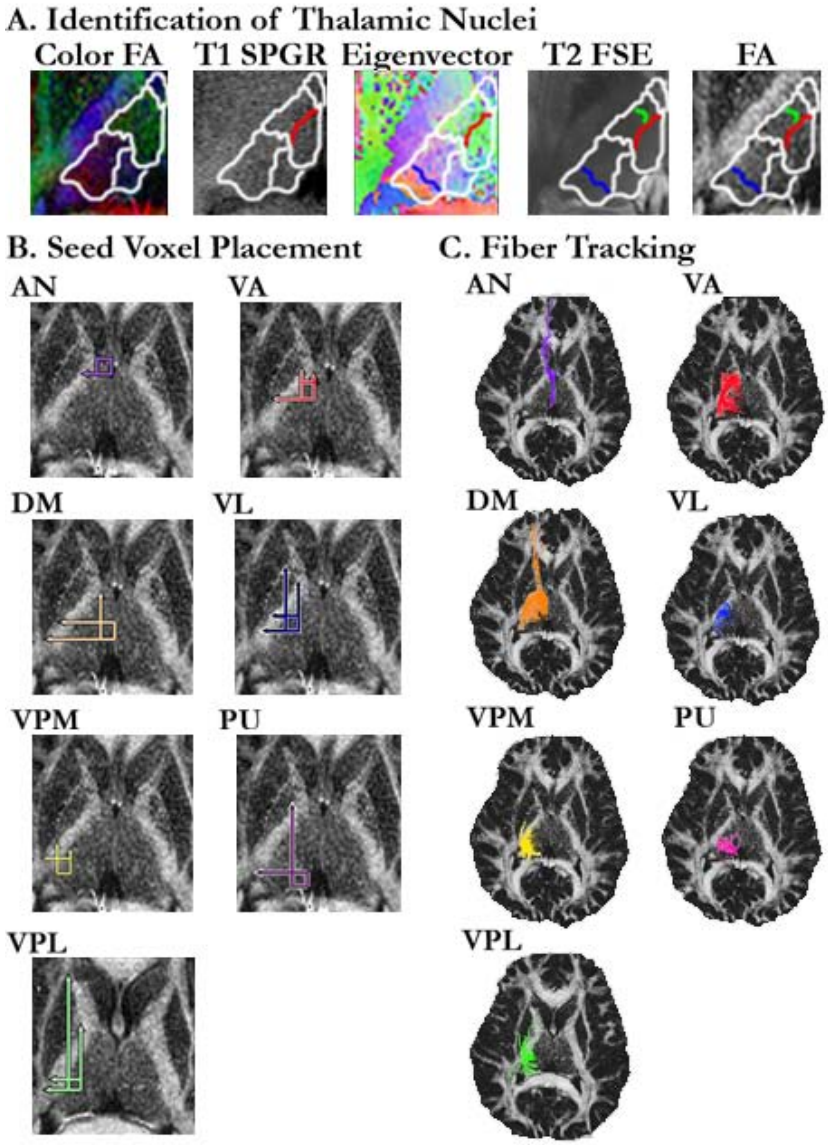

Figure 4. Thalamic nuclei and location of nuclei as well as identified fiber projections.

Results. Relative to controls, patients with a history of brain injury showed reductions in fractional anisotropy in both the anterior and posterior corona radiata, forceps major, the body of the corpus callosum and fibers identified from seed voxels in the anterior and ventral anterior thalamic nuclei. Fractional anisotropy from cortico-cortico and corpus callosum regions of interest did not account for significant variance in neuropsychological function. However, fractional anisotropy from the thalamic seed voxels did account for variance in executive function, attention, and memory. Scatter plots and regression lines indicating these relationships are presented below in Figure 5.

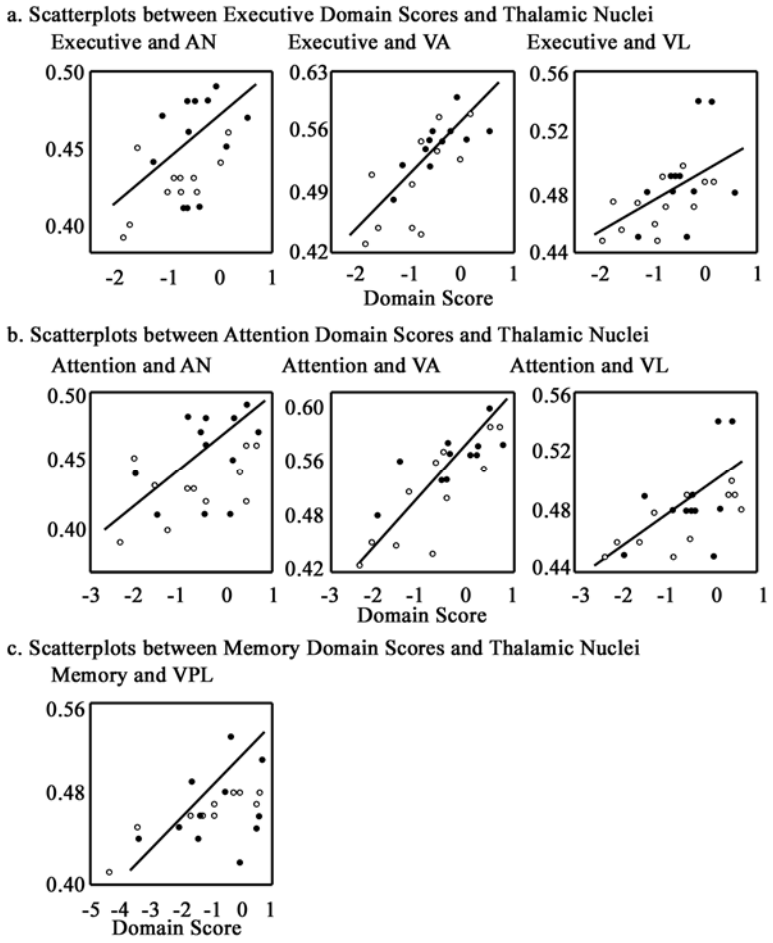

Figure 5. Relationship between fractional anisotropy extracted from thalamic nuclei and neuropsychological testing for mild (open circles) and moderate (black) TBI.

Conclusions. The data provide preliminary evidence that traumatic brain injury and resulting diffuse axonal injury results in damage to the thalamic projection fibers and is of clinical relevance to cognition.

Preliminary Investigations of Caudate Integrity in TBI

For the role of the caudate, we have now placed regions of interest in 3 locations of the head of the caudate in each hemisphere. The reason for investigating the caudate is two fold. First, caudate lesions are common in TBI. Second, the caudate is a major component of the dopamine system and regulates dopamine release. As dopamine is thought to be a major

component in mood disorders and mood disorders are common we set out to examine the relationship between DTI measure of caudate integrity and mood in TBI.

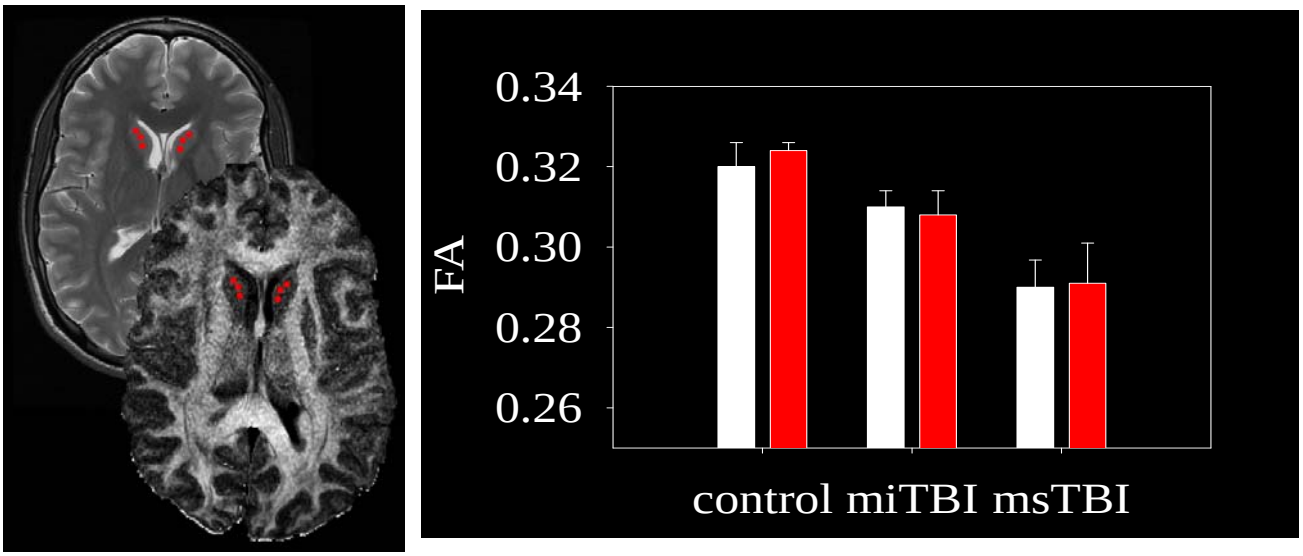

Figure 6. Locations of caudate regions of interest (left) and resulting fractional anisotropy data for 5 control subjects, 5 mild TBI, and 5 moderate TBI.

As can be seen in Figure 6, there is some preliminary evidence to suggest that there is damage to the caudate in TBI. We will now move forward and have a second rater also draw regions of interest and apply this to the remaining subjects.

Preliminary Investigations of Cerebeller Injury in TBI

We are also in the very beginning stages of analysis of cerebeller data. Like the caudate, the cerebellum is believed to support mood as well as most aspects of cognition. Placement of these regions of interest have been challenging given the high number of crossing white matter fibers in TBI. Within the last month we have validated the methods and will now begin applying these methods to patient data. Specific regions of interest are indicated below in Figure 7.

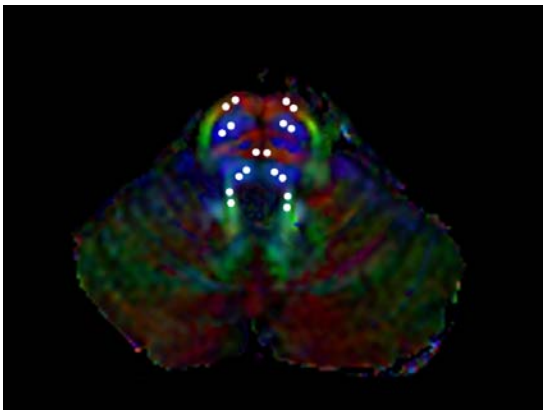

Figure 7. Locations of cerebeller regions of interest including the left and right superior cerebeller peduncle, the left and right inferior peduncle, the middle cerebeller peduncle, the left and right cortico-spinal tract, and the transverse pontine fibers.

In summary, we have accomplished each task within our scope of work and have developed new methods that can be applied to the data. Our subject recruitment is on-task. We hope to increase subject recruitment in the coming year to allow more focus on the data analysis. We look forward to the opportunity of continuing this work in the year ahead.

Key Research Accomplishments

1. Obtainment of approval for human subjects research at both the institutional and Army levels.
2. Validation of pulse sequences for data collection.
3. Collection and use of quality assurance data to identify potential scanner problems that might have influenced quality. By identifying problems before the personnel at the MRI center we potentially reduced the likelihood for poor data quality.
4. Development and validation of methods for assessment of thalamic fiber integrity.
5. Preparation of a manuscript which received positive reviews at a top journal.
6. Invitation for submission of a manuscript to describe effects of head injury using radiologic tools.

Reportable Outcomes

Abstracts and Talks

Little DM, Kraus MF, Zhou XJ, Joseph J*, Susmaras T*, Geary EK, Pliskin N, Gorelick P. High-resolution diffusion tensor imaging of thalamic projection fibers in TBI. International Neurotrauma Society Meeting, Santa Barbara, CA 2009.

Little DM, Kraus MF, Joseph J, Geary EK, Susmaras T, Zhou XJ, Gorelick PB. Thalamic projection fibers and cognitive impairment following traumatic brain injury. Department of Defense Military Health Research Forum. Kansas City, MO 2009.

Manuscripts In Press or Under Review (included as Appendices)

Little DM, Kraus MF, Joseph J*, Geary EK, Susmaras T*, Zhou XJ, Pliskin N, Gorelick PB. Thalamic integrity underlies executive dysfunction: Evidence from Traumatic Brain Injury. Under review, *Neurology*.

Little DM, Kraus MF, *Jiam C, *Moynihan M, *Siroko M, *Schulze E, *Geary EK. Imaging hypoxic-ischemic brain injury. *NeuroRehabilitation* (In Press).

Conclusion

The results of the work accomplished in year 1 are significant. First, we have provided data to suggest that there is a central mechanism of cognitive impairment in TBI. If validated by other laboratories this has the potential to change treatment approaches and assessment of treatment validity. This impression was supported by the enthusiastic reviews obtained from the thalamic manuscript. Reviewer 2 indicated that the findings “provide a significant and very important advance in the field of traumatic brain injury.” The significance of these findings does not end

with the publication of this manuscript. If the thalamus is in fact a central mechanism then one would believe that the brain stem and cerebellum are also highly likely targets and may explain sustained post-concussive symptoms in TBI.

References

None.

Appendix 1

Little DM, Kraus MF, Joseph J*, Geary EK, Susmaras T*, Zhou XJ, Pliskin N, Gorelick PB. Thalamic integrity underlies executive dysfunction: Evidence from Traumatic Brain Injury. Under review, *Neurology.*

NEUROLOGY/2009/294231

Thalamic Integrity Underlies Executive Dysfunction in Traumatic Brain Injury

Deborah M. Little PhD [1-3,7,8], Marilyn F. Kraus MD[1,4,8], Josh Joseph BS[1,7], Elizabeth K. Geary PhD [1,4,7], Teresa Susmaras BA [1,7], Xiaohong Joe Zhou PhD [5,6,9], Neil Pliskin PhD [4,8], and Philip B. Gorelick MD, MPH[1,7]

From the Departments of Neurology[1], Anatomy[2], Ophthalmology[3], Psychiatry[4], Neurosurgery and Radiology[5], and Bioengineering[6], and from the Centers for Stroke Research[7], Cognitive Medicine[8], and MR Research[9] at The University of Illinois Medical Center at Chicago; Chicago Illinois 60612 USA.

Corresponding Author:
DM Little; 1645 West Jackson Suite 400, Chicago, Illinois 60612; Email: little@uic.edu, Phone: 312.355.5404, Fax: 312.355.5444

Abstract Word Count: 240
Title Character Count (with spaces): 76
Total Word Count (not including abstract, references, figure captions): 2906

Acknowledgements
This work is supported in part by a Department of Defense/Congressionally Directed Medical Research Program grant PT 075675 grant (DML), NIH grant K23 MH068787 from the National Institute of Mental Health (MFK), the Marshall Goldberg Traumatic Brain Injury Fund (MFK) and a grant from the Chicago Institute for Neurosurgery and Neuroresearch Foundation (DML). The contents of this paper are solely the responsibility of the authors and do not necessarily represent the official views of the University of Illinois at Chicago, Department of Defense, or the National Institute of Mental Health. The authors also are grateful to Robert Sekuler (Brandeis University), Lisa Connor (Washington University), Alan Hartley (Scripps College), and Margret Malloy (Vista Partners) for their helpful comments on previous versions of the manuscript.

Disclosure
This study was sponsored by grants from the Department of Defense, National Institute on Mental Health, and the CINN Foundation.
Dr. Little is funded by Department of Defense/Congressionally Directed Medical Research Program grant PT 075675, NIH grant AG028662 and received research support from the CINN Foundation.
Dr. Kraus is funded by NIH grant MH068787.
Dr. Zhou is funded by NIH grant AG028662 and DOD grant PT 075675.
Dr. Geary, Mr. Jacobs and Ms. Susmaras report no disclosures.
Dr. Gorelick is an adjudication committee member for Abbott, Pfizer, Posen, Savient, and TAP/Takeda, a consultant for InTouch Health, BMS/Sanofi, and Easai, and a member of the steering committee for Bayer, Boehringer Ingleheim, and Brainsgate.

Abstract

Objective. To quantify the effects of traumatic brain injury on integrity of thalamo-cortical projection fibers and to evaluate whether damage to these fibers accounts for impairments in executive function in chronic traumatic brain injury

Methods. High-resolution (voxel size: 0.78mmx0.78mmx3mm^3) diffusion tensor magnetic resonance imaging of the thalamus was conducted on 24 patients with a history of single, closed-head traumatic brain injury (12 each of mild TBI and moderate to severe TBI) and 12 age- and education- matched controls. Detailed neuropsychological testing with an emphasis on executive function was also conducted. Fractional anisotropy was extracted from 12 regions of interest in cortical and corpus callosum structures and 7 subcortical regions of interest (anterior, ventral anterior, ventral lateral, dorsomedial, ventral posterior lateral, ventral posterior medial and pulvinar thalamic nuclei).

Results. Relative to controls, patients with a history of brain injury showed reductions in fractional anisotropy in both the anterior and posterior corona radiata, forceps major, the body of the corpus callosum and fibers identified from seed voxels in the anterior and ventral anterior thalamic nuclei. Fractional anisotropy from cortico-cortico and corpus callosum regions of interest did not account for significant variance in neuropsychological function. However, fractional anisotropy from the thalamic seed voxels did account for variance in executive function, attention, and memory.

Conclusions. The data provide preliminary evidence that traumatic brain injury and resulting diffuse axonal injury results in damage to the thalamic projection fibers and is of clinical relevance to cognition.

Traumatic brain injury (TBI) is a serious public health problem with a high incidence [1-3] which can result in structural damage to the cerebrum including contusions, edema and diffuse axonal injury (DAI)[4]. DAI has been demonstrated in all stages and severities [5-7] and is often the only significant pathology in milder injury [6, 8-15]. The variable nature of injury mechanism, severity, lesion presence and location makes the identification and definition of the key cerebral mechanisms which underlie behavioral impairments challenging. Behaviorally, patients with a history of TBI commonly have deficits in cognition, behavior and mood that load heavily on the executive or frontal lobe functions [16-20]. However, the relationship between measures of frontal lobe structure and shearing within frontal lobe white matter tracts and cognition are generally weak [7, 19, 21]. This weak relationship between frontal structure and function, coupled with the finding that DAI not only affects local function but can also disrupt critical cortical-subcortical pathways [22, 23], led us to the general hypothesis that damage to cortical-subcortical fibers projecting to and from the thalamus contribute to chronic impairment in cognition and behavior. This hypothesis is supported by the report that thalamic volume is related to 2 year outcome [24]. We tested the hypothesis that damage to thalamic projection fibers underlies executive function impairments using high-resolution diffusion tensor imaging of the thalamus (DTI) in a group of healthy controls and in two groups of patients who had sustained a closed-head brain injury.

Methods

Standard Protocol Approvals, Registrations, and Patient Consents

The research was conducted with in compliance with both institutional (University of Illinois at Chicago) and federal (Department of the Army) human subjects guidelines using standards consistent with the declaration of Helsinki. All subjects provided prospective, written, informed consent.

Participant Characteristics

A total of 24 patients with a history of a single, closed-head type TBI were recruited via advertisements in local papers (no patients were recruited from an active clinical practice) and were screened and consented in the order they responded to advertisements. Inclusion criteria for patients and controls included age at study (18-50 years of age included), education (at least one year of high school), negative history (prior to TBI) for psychiatric illness, and English as a native language. For

TBI patients, age at injury was required to be after age 16 and at least 12 months prior to study. Patients were classified as having had a mild TBI (miTBI) if they reported either no loss of consciousness (LOC) or a LOC less than 30 minutes and post-traumatic amnesia (PTA) for less than 24 hours. Patients were classified as moderate to severe TBI (msTBI) if they experienced LOC greater than 30 minutes, PTA greater than 24 hours, or a positive MRI or CT study for contusion, edema, or ischemia at the time of injury. Detailed clinical assessments were carried out (MFK) to establish injury severity and extract specific injury variables including mechanism of injury, presence and duration of LOC, neurologic exam, presence of post-traumatic headache and associated injuries at the time of TBI were recorded. See Supplemental Data Table e1 for details. Estimates of PTA and LOC are presented as the nature and time from injury makes accurate estimates difficult. Subjects were excluded if they were taking any medications used to enhance cognitive function, significant depressive symptoms, current or past litigation related to the injury, or failure on tests of effort and symptom validity. All but two of the TBI had returned to work or school following the injury. Of the two, one was unable to return to work and the other dropped out of college. The gross majority of subjects reported a level of function less than prior to the injury (20 of 24) even though more than 14 returned to the same job or matriculated to the next stage of schooling. Of the 24 TBI, all but three reported some degree of sustained problems with cognition or sustained alteration in cognitive function at the time of testing. In terms of alterations in behavior, 12 of the 24 reported sustained alterations in behavior following the TBI.

The groups were matched on age and education with controls reporting 15 years of formal education (M=15.4, SEM=0.6) and were 31 years of age (M=30.8, SEM=3.04); miTBI reporting16 years of formal education (M=16.4, SEM=0.36) and age at study of 31 years (M=31.2, SEM=2.71) and msTBI 16 years of formal education (M=16.1, SEM=0.60) and 33 years of age (M=33.3, SEM=3.20). The miTBI and msTBI were roughly matched for age at injury (miTBI: M=27.2 years of age, SEM=2.4; msTBI: M=25.3 years of age, SEM=2.9). All three groups were matched on estimates of premorbid IQ (controls: M=112.4, SEM=3.55; miTBI: M=111.2, SEM=2.78; msTBI: M=111.7, SEM=1.6).

Statistical Analyses

Neuropsychological test scores were analyzed using a one-way ANOVA with group membership (controls, miTBI, msTBI) as the between subjects factor and were corrected for multiple comparisons using the least significant difference post-hoc tests. The primary measures of interest were 3 scores which were each a composite of those individual test results which loaded preferentially on executive, memory and attention domains. Group differences on individual neuropsychological tests were corrected for multiple comparisions using the Bonferroni correction. The primary analyses carried out on the dependent measures extracted from the DTI data was a one-way mixed design ANOVA with group membership (controls, miTBI and msTBI) as the between subjects factor. The primary dependent measure was fractional anisotropy (FA). Data were confirmed to have a normal distribution using the Kolmogorov-Smirnov test. To examine the relative contributions of thalamic and cortical (to include cortico-cortico and corpus callosum white matter) regions of interest, both bivariate correlations and stepwise linear regressions were used.

Neuropsychological Testing

Subjects completed a neuropsychological battery comprised of tests known to be sensitive to the cognitive deficits associated with TBI, with a focus on tests of executive function, attention, memory and processing speed. Additional measures were included to assist in the estimation of premorbid function and to assess effort. Tests and selected scores from the tests are included in Supplemental Data Table e1. These test scores were converted to standardized z scores (based upon control means) and combined to create three cognitive domains (Executive, Attention, Memory).

Image Acquisition

In order to reliably perform the FA analysis and fiber tracking in the thalamus we used a customized high resolution DTI protocol which relied on a single-shot EPI acquisition[25] together with parallel imaging using an 8-channel phased-array head coil on a GE 3.0 T Signal HDx scanner (General Electric Healthcare, Milwaukee, Wisconsin). The imaging parameters included: TR/TE=5000/64ms, b=0,1000 s/mm^2, diffusion directions=27, FOV=20x20cm^2, matrix=256x256, slice thickness/gap=3/0mm, slices=7, NEX=8, and acceleration factor=2. In order to visualize the thalamus and differentiate the thalamus from surrounding structures a set of 2D T2-weighted images were acquired (fast spin echo (FSE), axial, TR/TE=4000/80ms, ETL=8, matrix=512x256, FOV=20x20cm^2, slices=7, slice thickness/gap = 3/0 mm). To visualize the dorsomedial nucleus, 3D inversion recovery spoiled gradient recalled echo (3DIRpSPGR) images were acquired (TR/TI/TE=13.8/600/2.7ms, flip angle=25°, matrix=512x192, FOV=22x16cm^2, slices=120, slice thickness=1.5mm, NEX=1, bandwidth=±15.6 kHz).

Diffusion Tensor Imaging and Analysis

DTI is a type of diffusion-weighted imaging that allows the assessment and visualization of large white matter fibers on a millimeter-level multidimensional scale. DTI takes advantage of the diffusivity of water and the restrictions imposed on the diffusion of water by white matter fiber tracts. When fiber tracts are dense the restriction imposed by their density leads to directionally dependent or anisotropic diffusion with the shape of water diffusion occurring preferentially along those tracts. When there is less organization or a lack of aligned and organized fiber structures (i.e., gray matter, cerebrospinal fluid, axonal loss or demyelination) the shape of water diffusion will be more isotropic. Commonly, the degree of alignment and anisotropy is calculated as the fractional anisotropy (FA). FA values range from 0 to 1, where 0 represents isotropic diffusion and 1 represents anisotropic diffusion.

In the present study, the diffusion images were reconstructed and FA calculated using DTI Studio[26]. For each slice, the set of 28 DTI images were examined for image quality. Head movement was required to be within one voxel across the image acquisition. Because noise can introduce bias in estimates of the eigenvalues and decrease the signal-to-noise ratio, a background noise level of 125 (MR Units) was applied prior to calculation of pixel-wise FA, eigenvectors, and eigenvalues. All region of interest analyses were carried out on each individual in original image space.

Effects of Trauma on Cerebral White Matter

To assess the effects of trauma on DTI three analyses were applied. Gross measures of whole brain FA and thalamic FA were extracted. For the whole brain mask each voxel with an FA greater than 0.2 was included (ensuring only white matter in the calculations). Second, specific regions of interest (ROI) were drawn on corpus callosum and cortico-cortico white matter tracts which have been previously implicated in head injury [7]. These “cortical” ROIs were placed on the cortical-spinal tract (CST), anterior corona radiata (ACR), posterior corona radiata (PCR), forceps minor (fMin) and forceps major (fMaj), sagittal stratum (SS), internal capsule (IC), inferior frontal occipital fasciculus (IFOF), superior longitudinal fasciculus (SLF), and in the genu (gCC), body (bCC), and splenium (sCC) of the corpus callosum. Separate ROIs were placed in the left and right hemisphere where appropriate. Details on placement can be found in the Supplemental Data.

Finally, fiber tracking was used to assess damage to the fibers projecting from the thalamus. Seed voxels (small regions of interest) were placed in seven thalamic regions (shown in Figure 1) including the anterior thalamic nucleus (AN), ventral anterior thalamic nucleus (VA), ventral lateral thalamic nucleus (VL), dorsomedial nucleus (DM), ventral posterior lateral nucleus (VPL), ventral posterior medial nucleus (VPM), and pulvinar (PU). The purpose of these seed voxels is to identify all fiber tracts which run through this region. FA can then be extracted from these fibers identified by the seed voxels and fiber tracking from these seeds. Inter-rater reliability was greater than 0.94 for

placement of AN, VA, DM, VL, and PU seed voxels. Inter-rater reliability was 0.85 for VPL and VPM. Specific details and rules for placement are included in the Supplementary Material.

Results

Behaviorally, patients with a history of TBI performed worse on measures of executive function relative to controls [$F(2,36)=5.15$, $p= 0.011$, $\eta^2=0.26$]. Although there were trends for reduced attention and memory performance in TBI, neither of these comparisons reached significance. These findings are consistent with previous work from our group and the literature in general[7, 27-29]. A detailed list of performance for each subject group on each test can be found in Supplemental Data Table e1.

There was an overall effect of subject group (controls, miTBI, msTBI) on FA in the ACR [$F(2,36)=9.71$, $p< 0.001$, $\eta^2=0.0.37$], PCR [$F(2,36)=3.91$, $p=0.030$, $\eta^2=0.19$], fMaj [$F(2,36)=5.07$, $p=0.012$, $\eta^2=0.23$], and in the bCC [$F(2,36)=4.002$, $p=0.028$, $\eta^2=0.20$] with the greatest differences between controls and those with more severe injury (msTBI; see Figure 2A). The patients did not differ from controls in the remaining cortical regions of interest. Nor did they differ in whole brain FA. There was an overall effect of subject group on thalamic FA [$F(2,36)=5.40$, $p=0.009$, $\eta^2=0.25$] with controls having higher FA in the thalamus than msTBI. Although there was a trend for the miTBI to show reduced FA relative to controls in thalamic FA the comparison did not reach significance.

Comparisons between groups on FA extracted from the seed regions in the thalamic nuclei are presented in Figure 2B. There was an effect of subject group only in fibers extracted from the AN [$F(2,36)=5.82$, $p=0.007$, $\eta^2=0.26$] and VA [$F(2,36)=4.82$, $p=0.015$, $\eta^2=0.23$] seed voxels. Post-hoc comparisons between controls, miTBI, and msTBI are also indicated on Figure 2B.

To examine the relationship between cognition and fiber tract integrity, a series of bivariate correlations were conducted. All of the ROIs were included and examined relative to the neuropsychological domain scores for executive function, memory function, and attention. Correlations were conducted for the control and TBI separately so as not to bias the correlation simply because patients show lower FA than controls.

For controls, there was a statistical relationship between the executive domain score and FA of the gCC (gCC) [$r=0.685$, $p=0.014$] as well as FA of fibers identified with the VL seed voxel [$r=0.586$, $p=0.045$]. The attention domain scores were also correlated with FA from the VL [$r=0.668$, $p=0.018$] and VPL [$r=0.639$, $p=0.025$]. Memory function in controls was associated with FA in the genu of the gCC [$r=0.667$, $p=0.018$] and inferior frontal occipital fasciculus [$r=0.605$, $p=0.037$].

Scatterplots of the significant correlations between neuropsychological function and FA for the TBI are presented in Figure 3. In the TBI groups, there were no correlations between any cortical or corpus callosum ROIs with executive function, attention, or memory performance. There was a relationship between the attention domain and FA in the gCC [$r=0.506$, $p=0.012$]. For thalamic seed voxels, executive function was related to FA extracted from seed voxels in the AN [$r=0.497$, $p=0.014$], VA [$r=0.741$, $p<0.001$], and VL [$r=0.540$, $p=0.006$]. Similar relationships were also found between the attention domain score and integrity of fibers from the AN [$r=0.489$, $p=0.015$], VA [$r=0.786$, $p<0.001$], and VL[$r=0.523$, $p=0.009$]. In contrast, memory function was associated with integrity of VPL fibers [$r=0.540$, $p=0.006$]. Integrity of DM was not associated with memory function.

We also examined the injury variable duration of loss of consciousness relative to FA measures and relative to domain scores. Accurate ranges of LOC were collected for 19 of 24 subjects. The remaining subjects reported LOC but did not have a witness present. Duration of LOC was

negatively correlated with the executive domain (r=-0.460, p=0.048), memory domain (r=-0.500, p=0.029). LOC also correlated with FA from the bCC (r=-0.661, p=0.002).

Because of a significant amount of shared variance between nuclei a series of linear regressions were applied to the TBI data with the executive function domain score as the dependent variable. In the first stepwise linear regression, the frontal lobe ROIs including the ACR, fMin, and the gCC were entered. This model did not account for the executive domain variance [r^2=0.19, p=0.236]. Because the white matter tracts are not contained within the frontal lobe we expanded this regression to include any ROIs which have fiber projections to or from the frontal lobes. This model was expanded to include not only the ACR, fMin, gCC but also the CST, SS, and IFOF. Although this model accounted for more variance than the first model, it still did not reach significance [r^2=0.322, p=0.291]. This same strategy was applied to the fiber projections from the thalamic nuclei. The projections from the AN, VA, VL, and DM were entered into a linear regression with executive function as the dependent measure. This model did account for variance in the executive domain [r^2=0.674, p<0.001]. Within this model, the only unique predictor was FA from the VA seed voxels [p=0.001] with VA accounting for 26% of the unique variance. Duration of LOC was also added into the regression models. Although it accounted for additional variance in the sub-cortical model [r^2=0.701, p<0.001], LOC on its own was not a significant unique predictor.

Discussion

The present study presents preliminary support for a thalamic hypothesis as a central mechanism of injury and resultant cognitive impairment in TBI. The thalamus, although not located near the skull and therefore less susceptible to direct contusion, is likely differentially sensitive to shear and strain injury because of the corticospinal fibers which extend from the spine to the cortex. Within the thalamus, incoming sensory, motor, and cognitive processing pathways are organized and integrated within distinct nuclei. Following this integration, various thalamic nuclei send diffuse and specific efferent projections to cortical, cerebellar, and subcortical regions. The thalamus is also known to gate and mediate many cognitive, sensory, motor, and behavioral functions and damage to these projection fibers can result in wide-spread functional impairments[31]. Overall, thalamic lesions are associated with a decrease in executive function with larger lesions associated with greater deficits [32, 33]. In the case of frontal lobe functions, impairments in executive function could be accounted for by damage to the fiber projections to and from the dorsomedial nucleus, anterior thalamic or ventral anterior thalamic nuclei rather than the frontal lobes per se.

However, because the thalamus is a relay center for the majority of cortical fiber projections, characterization of thalamic damage must include assessments of the integrity not only of thalamus proper but also for fibers entering or exiting the thalamic nuclei. The fiber tracking methods employed here with the spatial resolution provided by the sequences used allow this concern to be addressed. These projection fibers may in fact be even more susceptible to TBI than the thalamus itself because of the sharp turning angles of the cortical-subcortical fibers both as they leave the thalamus and again as they enter the cortex [22, 23].

The present data reaffirm the presence of executive dysfunction in TBI and suggest that executive dysfunction is correlated with cortical-subcortical damage rather than simply due to damage to the cortical frontal lobe structures, cortico-cortico tracts, or corpus callosum alone. This conclusion is supported both by the presence of correlations between executive function and FA in thalamic nuclei and also by the absence of correlations with FA in the measured cortical regions. The data do not however identify the location of damage within these fiber tracts. The primary damage to these fibers could occur at the boundary of the thalamus as the fibers exit the thalamus or it could occur at the junction of gray and white matter as the fibers enter the cortex.

Although these conclusions are based upon a relatively small sample (n=24) the data do suggest that thalamic integrity may be a central mechanism in TBI and provide initial evidence that damage to thalamic projection fibers, especially those involved in frontal-thalamic circuitry, is of great importance in understanding executive dysfunction following TBI. Furthermore, the findings support the need for further investigation into the applicability of these measures in other populations which demonstrate executive dysfunction.

Figure Captions

Figure 1. Thalamic nuclei. Seed regions for the VPL (green), AN (purple), VA (red), DM (orange), VL (blue), VPM (yellow), and PU (pink) overlaid on the T2-weighted images.

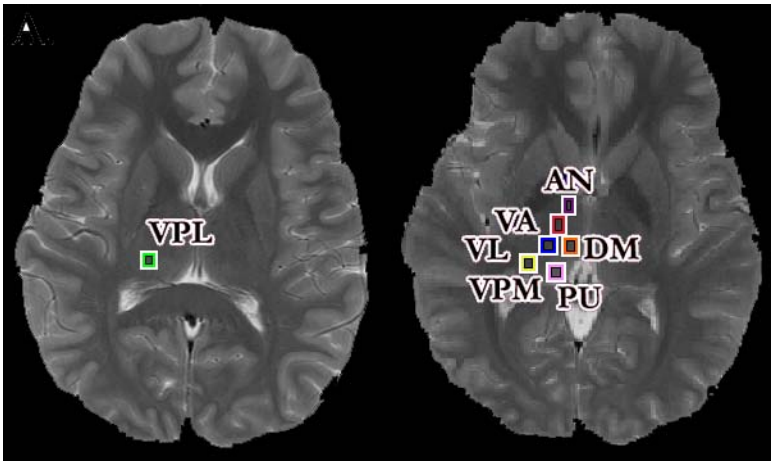

Figure 2.Average cortical and subcortical FA. Mean FA extracted from the ACR, PCR, fMaj and bCC as well as from the thalamus and from fibers identified from seed regions in the AN and VA Significant post-hoc comparisons between groups are indicated (* $p<0.05$; ** $p<0.01$). Cortical in this figure refers to regions of interest that include cortico-cortico tracts and regions in the corpus callosum.

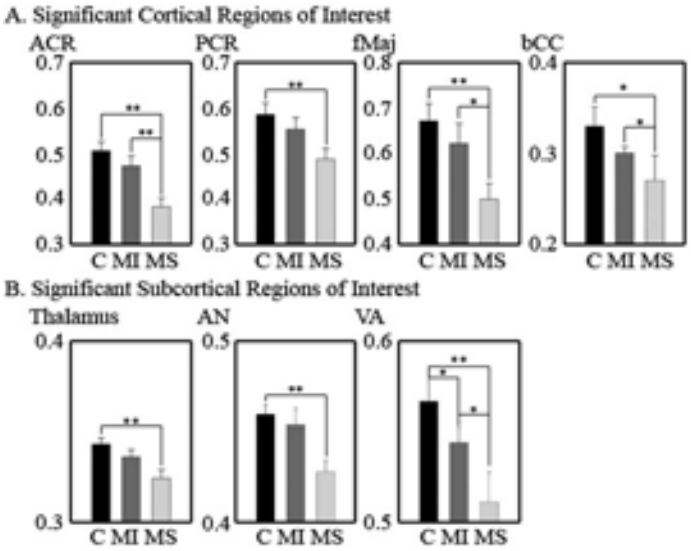

Figure 3. Relationship between thalamic FA and cognition. Scatterplots of FA from thalamic seed voxels relative to executive (A), attention (B), and memory (C) domain scores for TBI patients. Best-fit lines are indicated in gray. Unfilled circles represent mild TBI while filled circles represent moderate to severe TBI.

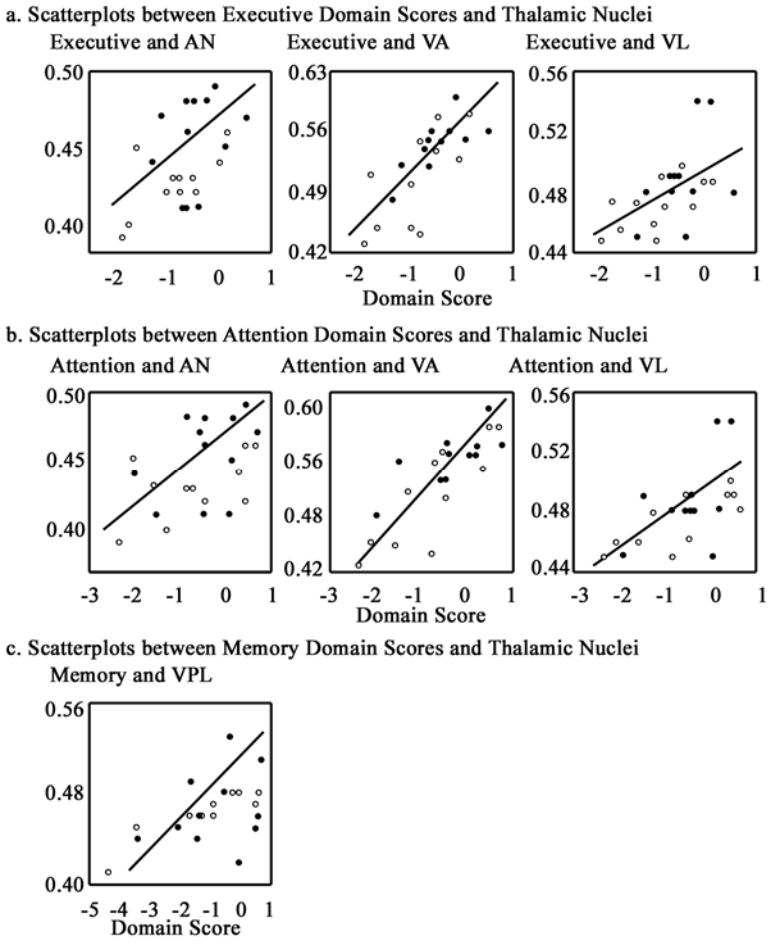

Supplemental Data

Methods

Injury Characteristics

Detailed clinical assessments were carried out (MFK) to establish injury severity and extract specific injury variables including mechanism of injury, presence and duration of LOC, neurologic exam, presence of post-traumatic headache and associated injuries at the time of TBI were recorded. These data are presented for each TBI subject in Table e1.

Placement of cortical ROIs

Regions of interest were drawn in the cortical-spinal tract (CST), anterior corona radiata (ACR), posterior corona radiata (PCR), forceps minor (fMin) and forceps major (fMaj), sagittal stratum (SS), internal capsule (IC), inferior frontal occipital fasciculus (IFOF), superior longitudinal fasciculus (SLF), and in the genu (gCC), body (bCC), and splenium (sCC) of the corpus callosum. Separate ROIs were placed in the left and right hemisphere where appropriate. Figure e1 provides information as to the specific location of these ROIs on a single subject. These ROIs were drawn with reference to the color-coded FA and T2 image for each subject and with reference to a DTI atlas. [1] Each ROI, with the exception of the external capsule, had an area of $15mm^3$. Because of the width of the external capsule, the IC ROI had an area of $10mm^3$. The bCC ROI was placed on the slice in which the body of the left and right superior branches of the corpus callosum met in the mid-sagittal slice (see Figure e1A). On this same axial slice, the ACR, SLF, PCR, and CST were drawn. The CST was placed in the posterior limb 20mm posterior to the edge of the bCC ROI. The ACR was placed 15mm anterior to the intersection of the corpus callosum with the CST. The PCR was placed 15mm posterior to the posterior intersection of the CST and CC. The SFL was placed lateral and anterior to the bCC ROI. The gCC and sCC were placed on the axial slice which clearly showed both the internal and external capsules. These were placed at midline. The IC, EC, and SS were placed on the same axial slice as used for the gCC and sCC in all subjects. The EC was placed in the middle of the posterior aspect of the EC whereas the IC was placed midway (anterior to posterior) between the intersection of the IC and EC at the location where the EC was most lateral to the edge of the brain. Finally, the fMin, fMaj, and IFOF were drawn on the slice through which the anterior commissure was visible on the T2 image. The fMin was placed anterior and lateral to the boundary of the corpus callosum. The fMaj was placed posterior and lateral to the posterior boundary of the corpus callosum. The IFOF was located lateral and anterior to the fMaj.

Anatomical Localization of Thalamic Nuclei

Although the thalamic nuclei have distinct cytoarchitectural boundaries, differentiation of these borders in vivo has been challenging. Recent reports with DTI suggest that the boundaries of the large nuclei can be differentiated based upon fiber orientation. In other words, because the projection of fibers from the thalamic nuclei are so well defined, one can use homogeneity of primary eigenvectors within nuclei to help define their boundaries [2,3]. However, the DM can not be differentiated using these methods. However, the DM can be differentiated from other nuclei based upon tissue relaxation times using T1 imaging with inversion recovery.

To begin our analyses, we first co-registered all images to the color-coded FA maps using MRI View (DTI Studio, Johns Hopkins). To ensure correct anatomical localization the boundaries of the thalamus, we used the color-coded FA maps to delineate the boundaries of the thalamus. The thalamus was defined laterally by the internal capsule, medially by the third ventricle, superiorly by the caudate and lateral ventricles, and inferiorly by the brain stem. All of these boundaries are easily observed on the color-coded FA maps. Additionally, the color-coded FA maps allow differentiation

of the AN and PU. The anterior border of VA, DM and the posterior boundary of VL were identified from the color-coded maps (see Figure e2). These boundaries were then applied to the T1-weighted images on which the boundary of DM was drawn based upon differences in signal intensity between the DM (red line) and ventral portions of the thalamus. [4] These boundaries were then applied to the primary eigenvector maps. Similar colors on the primary eigenvector map indicate that nearby voxels share the same primary eigenvector. From this map the posterior boundary of the VA was identified (blue line). These were then applied to the T2 weighted FSE which allowed visualization of the anterior boundary of the VL (and posterior boundary of the VA) (green line). From these rough boundaries, rules guiding seed voxel placement within each nucleus were created.

Seed Voxel Placement

In addition to ensuring that seed voxels were placed in the correct anatomical location within the thalamus, our methods for placing seed voxels allowed for a high degree of reproducibility within our laboratory (inter-rater reliability > 0.94 for AN, VA, DM, VL, and PU and 0.85 for VPL, VPM). We did not use the entire boundary identified based upon geographic borders but instead placed a small seed voxel in the middle of each region. We acknowledge that some fibers identified by the seed region within a specific nucleus may include fibers from other nuclei. This is especially relevant for the VA, VPL, and VPM. As such, our methods likely exclude innervations from other nuclei thus underpowering our assessment. However, we believe the methods do allow investigation into differential geographic vulnerability although they may not clearly differentiate between thalamic nuclei. Furthermore, some nuclei are innervated from multiple sources. However, for statistical reasons, we wanted to ensure that no single fiber would be calculated in multiple regions. This requirement reduced our sensitivity to those nuclei which are innervated from multiple sources. These seed voxels and rules guiding the placement of these voxels are indicated in Figure e2B.

Anterior Thalamic Nucleus (AN). The AN seed region was defined laterally by the internal capsule, medially by the edge of the thalamus, and anteriorly by the posterior edge of the caudate head and lateral ventricle. The posterior boundary for the seed voxel was defined by a horizontal line extending from the posterior edge of the anterior limb of the internal capsule. Any fiber which extended to the putamen or globus pallidus was excluded. Furthermore, any fiber which was also identified from seed voxels placed in the VA, VPL, VPM, DM, or PU were excluded. These criteria as well as the identified fibers from this seed voxel are identified in Figure e2B. The volume of the AN ROI was 14mm^3.

Ventral Anterior Thalamic Nucleus (VA). The anterior edge of the VA seed voxel was defined by a horizontal line extending from the anterior edge of the internal capsule and extended medially the width of the internal capsule. The VA extended posterior to a horizontal line drawn from the posterior boundary of the putamen. Any fibers which were indentified by the AN seed voxel were also excluded. The volume of the VA ROI was 16mm^3.

Ventral Lateral Thalamic Nucleus (VL). The VL seed region was defined medially by a vertical line drawn down from the medial edge of the bend of the internal capsule (the intersection between the anterior limb of the internal capsule and the body of the internal capsule), laterally by the edge of the internal capsule, anteriorly by a horizontal line extending from the posterior edge of the anterior limb of the internal capsule, and posteriorly by a horizontal line extending from the posterior boundary of the putamen. Fibers which were previously identified with either the AN or VA seed voxels were excluded. The volume of the VL ROI was 16mm^3.

Dorsal Medial Thalamic Nucleus (DM). The DM seed region was defined medially by the edge of the thalamic body, laterally by a vertical line extending from the posterior edge of the anterior limb of the medial edge of the internal capsule, posteriorly by a horizontal line extending from the posterior edge of the posterior limb of the internal capsule and anteriorly by a horizontal line

extending from the posterior edge of the putamen. Fibers which were previously identified with either the AN, VA, or VL seed voxels were excluded. The volume of the DM ROI was 16mm^3.

Ventral Posterior Medial Thalamic Nucleus (VPM). The VPM seed region was defined anteriorly by a horizontal line extending from the posterior edge of the putamen, laterally by a vertical line extending from the posterior intersection of the internal capsule and putamen, medially by a vertical line extending the intersection of the anterior limb of the internal capsule with the anterior edge of the putamen and posteriorly by the posterior edge of the thalamus. Fibers which were previously identified with either the AN, VA, VL, or DM seed voxels were excluded. The volume of the VPM ROI was 14mm^3.

Pulvinar (PU). A seed region was also placed in the pulvinar. This region was defined medially and posteriorly by the edge of the thalamus, laterally by a vertical line extending from the medial intersection of the anterior limb of the internal capsule and body of the internal capsule and anteriorly by a horizontal line extending from the intersection of the posterior limb of the internal capsule and putamen. Fibers which were previously identified with either the AN, VA, VL, DM, or VPM seed voxels were excluded. The volume of the PU ROI was 14mm^3.

Ventral Posterior Lateral Thalamic Nucleus (VPL). The seed region for the VPL was drawn on a slice 3mm anterior to the slide used for the other regions. This is because of its position lateral and anterior to the VPM. The anterior boundary of the VPL seed was a horizontal line extending from the intersection of the posterior limb of the internal capsule and putamen, laterally by a vertical line extending from the intersection of the anterior limb of the internal capsule and putamen, posteriorly by a horizontal line extending from the intersection of the putamen and posterior limb of the internal capsule and medially by the internal capsule. Fibers which were previously identified with either the AN, VA, VL, DM, VPM, or PU seed voxels were excluded. The volume of the VPL ROI was 14mm^3.

Results

Neuropsychological Test Results

Group means and comparisons between groups for each individual neuropsychological measure which contributes to the domain scores are presented in Table e2.

DTI Region of Interest Analysis and Descriptive Data

Means and standard deviations for each DTI region of interest are presented in Table e3. One-way ANOVA with group membership (controls, miTBI, msTBI) as well as pairwise comparisons and power estimates for each ROI are also included to the right of Table e3.

Additional Exploratory Correlations between DTI Variables and Individual Neuropsychological Measures

Because of significant variability across studies of TBI in both the neuropsychological test selection and correlations between neuropsychological tests and white matter, we conducted a series of exploratory correlations in the group of TBI subjects between our cortical and subcortical DTI measures and individual neuropsychological measures which together made up the composite executive domain scores. There were a number of correlations between cortical regions of interest and individual neuropsychological measures although no clear pattern emerged. These are summarized in Table e4A. Unlike for the cortical regions, integrity of fibers from the AN, VA, and VL loaded primarily and correlated significantly with the majority of measures that contributed to the executive domain scores. With the exception of the CPT hit reaction time measure all other executive measures correlated with at least one of these nuclei. These data are summarized in Table e3B.

Figure and Table Captions

Table e1. Injury characteristics for TBI patients. Abbreviations: MVA: motor vehicle accident, PMVA: pedestrian in MVA, LOC: loss of consciousness, PTA: post-traumatic amnesia, for neurologic exam: '-' negative, '+' positive, for radiologic finding: '++' acute findings via MRI or CT, '+' MRI finding at study.

Subject Number	Chronicity (months)	Mechanism of Injury	LOC	LOC (hours)	PTA (hours)	Neurologic Exam	PT Headache	Associated Injury	Radiologic Finding	TBI Severity
1	14	Athletic	-	0	<12	+	+	None	++	mild
2	134	Assault	+	<0.50	6	-	-	None	-	mild
3	91	Athletic	+	0.25	<12	-	+	Orthopedic	-	mild
4	34	MVA	+	<0.25	<12	-	+	None	-	mild
5	149	MVA	-	0	<5	-	-	Orthopedic	+	mild
6	29	Athletic	-	0	<12	-	-	None	-	mild
7	40	Athletic	+	<0.08	<12	-	+	None	-	mild
8	35	Athletic	-	0	<6	-	-	None	+	mild
9	87	Assault	+	<0.08	<12	-	-	None	-	mild
10	12	Athletic	-	0	40-48	-	-	None	-	mild
11	12	Assault	+	<0.02	<12	-	+	None	+	mild
12	29	P MVA	+	<0.02	10	-	+	Orthopedic	-	mild
13	15	MVA	+	288	---	+	-	Orthopedic	++	moderate
14	276	MVA	+	168	---	+	+	Orthopedic	++	moderate
15	197	Assault	+	>0.50	<72	-	+	None	+	moderate
16	13	P MVA	+	18-24	<168	+	-	None	-	moderate
17	62	MVA	+	144	---	+	+	Internal	++	moderate
18	106	P MVA	+	120	---	+	-	None	+	moderate
19	275	MVA	+	120	---	-	-	Internal	++	moderate
20	12	P MVA	+	120	---	+	-	Orthopedic	-	moderate
21	19	Athletic	+	0.25	1440	-	+	Internal	++	moderate
22	46	MVA	+	>0.50	168	-	+	None	+	moderate
23	14	MVA	+	11	840	-	+	Orthopedic	++	moderate
24	154	MVA	+	<48	48	-	+	None	-	moderate

Table e2. Neuropsychological test scores and comparisons between groups.

	Control		miTBI		msTBI		ANOVA		ANOVA		ANOVA		ANOVA
	Mean	SD	Mean	SD	Mean	SD	ctl, mi, ms		ctl, mi		ctl, ms		mi, ms
Executive Domain	**0.00**	**0.19**	**-0.49**	**0.13**	**-0.86**	**0.21**	**0.007**	******	**0.043**	*****	**0.006**	******	**0.149**
CPT Hit Reaction Time (msec)	365.88	80.61	357.48	69.98	370.90	83.53	0.914		0.788		0.882		0.674
Tower of London Total Moves	109.17	10.87	103.67	13.83	94.33	13.56	0.026	*	0.290		0.007	**	0.109
Stroop Color-Word (age-corrected)	46.25	12.13	42.42	7.30	43.17	13.04	0.673		0.358		0.555		0.864
PASAT Total	143.25	43.73	134.00	32.50	126.33	36.88	0.556		0.562		0.317		0.594
Trails B (seconds)	54.42	27.20	62.83	16.36	85.83	66.05	0.186		0.368		0.142		0.254
CPT Number of Comissions	12.08	7.13	13.92	7.55	15.67	7.95	0.515		0.547		0.257		0.586
COWAT Total	49.58	14.77	38.00	11.33	38.25	12.42	0.056		0.042	*	0.054		0.959
RUFF Unique Designs (t-score)	52.00	12.51	39.28	6.79	35.43	5.37	0.000	**	0.005	**	0.000	**	0.138
Digit Span Backward	9.08	2.19	7.50	2.39	6.92	2.02	0.059		0.105		0.020	*	0.526
Spatial Span Backward	9.00	1.41	8.58	1.62	7.58	1.73	0.097		0.509		0.039	*	0.158
Attention Domain	**0.00**	**0.26**	**-0.56**	**0.31**	**-0.83**	**0.39**	**0.115**		**0.127**		**0.068**		**0.341**
Digit Span Forward	11.75	2.56	10.92	3.00	11.25	2.56	0.753		0.472		0.637		0.772
Spatial Span Forward	10.00	2.09	8.75	2.01	8.58	2.11	0.202		0.149		0.112		0.845
Trails A (seconds)	20.25	7.56	26.83	10.05	41.50	37.50	0.080		0.083		0.067		0.204
CPT Number of Omissions	2.25	4.18	2.50	4.03	3.00	3.72	0.896		0.883		0.647		0.755
Memory Domain	**0.00**	**0.19**	**-0.46**	**0.22**	**-0.97**	**0.47**	**0.195**		**0.186**		**0.088**		**0.581**
CVLT Trials 1-5	58.00	7.01	53.42	11.61	49.67	10.97	0.143		0.254		0.037	*	0.425
CVLT Long-Free Recall	13.17	2.29	11.00	3.38	10.75	4.59	0.202		0.080		0.117		0.881
BVMT Trials 1-3	27.17	6.46	25.08	6.01	23.25	7.57	0.371		0.422		0.187		0.518
BVMT Delay Recall	9.75	2.22	9.08	2.27	8.67	2.71	0.546		0.475		0.296		0.687

*: p<0.05
**: p<0.01

Table e3. Descriptive and statistical comparisons for DTI data.

	Control		miTBI		msTBI		ANOVA		ANOVA		ANOVA		ANOVA	
	M	SD	M	SD	M	SD	c, mi, ms	η^2	c, mi	η^2	c, ms	η^2	mi, ms	η^2
Cortical ROIs														
ACR	0.51	0.07	0.47	0.08	0.38	0.07	0.000	0.37	0.280	0.05	0.000	0.48	0.005	0.30
CST	0.65	0.07	0.66	0.03	0.64	0.05	0.589	0.03	0.657	0.01	0.619	0.01	0.212	0.07
IC	0.67	0.03	0.66	0.03	0.65	0.06	0.629	0.03	0.449	0.03	0.402	0.03	0.717	0.01
IFOF	0.55	0.09	0.56	0.08	0.49	0.09	0.115	0.12	0.911	0.00	0.100	0.12	0.067	0.14
PCR	0.59	0.09	0.55	0.09	0.49	0.08	0.030	0.19	0.387	0.03	0.010	0.26	0.078	0.13
SFL	0.54	0.07	0.57	0.06	0.51	0.06	0.124	0.12	0.348	0.04	0.286	0.05	0.036	0.18
SS	0.58	0.06	0.57	0.08	0.56	0.07	0.774	0.02	0.693	0.01	0.460	0.03	0.763	0.00
fMaj	0.67	0.13	0.62	0.15	0.50	0.12	0.012	0.23	0.409	0.03	0.003	0.34	0.041	0.18
fMin	0.54	0.05	0.50	0.06	0.50	0.07	0.194	0.10	0.113	0.11	0.114	0.11	0.828	0.00
bCC	0.33	0.08	0.35	0.02	0.27	0.10	0.028	0.20	0.376	0.04	0.107	0.11	0.010	0.26
gCC	0.69	0.13	0.71	0.06	0.63	0.12	0.215	0.09	0.573	0.02	0.309	0.05	0.056	0.16
sCC	0.74	0.16	0.74	0.16	0.60	0.25	0.173	0.10	0.902	0.00	0.125	0.10	0.149	0.09
Thalamic Seed														
Thalamus	0.34	0.01	0.34	0.01	0.32	0.02	0.009	0.25	0.194	0.08	0.004	0.32	0.071	0.14
AN	0.46	0.02	0.45	0.03	0.43	0.02	0.007	0.26	0.585	0.01	0.001	0.41	0.027	0.20
DM	0.41	0.03	0.41	0.02	0.40	0.01	0.794	0.01	0.846	0.00	0.510	0.02	0.584	0.01
PU	0.42	0.03	0.42	0.02	0.42	0.02	0.830	0.01	0.569	0.02	0.742	0.01	0.771	0.00
VA	0.57	0.04	0.54	0.03	0.51	0.06	0.015	0.23	0.133	0.10	0.012	0.25	0.089	0.13
VL	0.50	0.04	0.49	0.03	0.47	0.02	0.162	0.11	0.520	0.02	0.069	0.14	0.161	0.09
VPL	0.48	0.05	0.47	0.03	0.46	0.02	0.543	0.04	0.540	0.02	0.301	0.05	0.627	0.01
VPM	0.44	0.05	0.45	0.04	0.44	0.02	0.897	0.01	0.843	0.00	0.813	0.00	0.577	0.01

Table e4. Correlations between individual neuropsychological measures and FA.

A. Cortical Correlations	**ACR**		**PCR**		**SS**		**IC**		**gCC**		**IFOF**		**SLF**	
	r	*p*	*r*	*p*	*r*	*p*	*r*	*p*	*r*	*p*	*r*	*p*	*r*	*p*
Executive Domain														
CPT Hit Reaction Time (msec)													-0.407	0.049
Tower of London Total Moves									0.594	0.002				
PASAT Total							-0.423	0.039	0.463	0.023				
Trails B (seconds)			-0.454	0.026	-0.413	0.045					-0.465	0.022	-0.408	0.048
RUFF Unique Designs (t-score)	0.431	0.035												
Attention Domain														
Spatial Span Forward	0.412	0.046							0.604	0.004				
Trails A (seconds)			-0.430	0.036	-0.424	0.039			-0.415	0.044	-0.490	0.015		

B. Thalamic Correlations	**AN**		**VA**		**VL**		**DM**		**VPL**		**VPM**		**PU**	
	r	*p*	*r*	*p*	*r*	*p*	*r*	*p*	*r*	*p*	*r*	*p*	*r*	*p*
Executive Domain														
CPT Hit Reaction Time (msec)													-0.413	0.045
Tower of London Total Moves			0.435	0.034										
Stroop Color-Word (age-corrected)	0.579	0.003	0.600	0.002	0.552	0.005								
PASAT Total	-0.494	0.014	-0.660	0.000	-0.451	0.027								
Trails B (seconds)			0.458	0.024										
CPT Number of Comissions			0.597	0.002	0.448	0.028								
COWAT Total	0.513	0.010												
RUFF Unique Designs (t-score)	0.430	0.036	0.558	0.005	0.545	0.006	0.419	0.041	0.399	0.053	0.404	0.050		
Digit Span Backward	0.423	0.040	0.513	0.010										
Spatial Span Backward			0.536	0.007	0.449	0.028			0.418	0.042				
Attention Domain														
Digit Span Forward	-0.439	0.032	-0.718	0.000	-0.475	0.019							0.426	0.038
Spatial Span Forward			0.615	0.001										
CPT Number of Omissions									0.532	0.008				
Memory Domain														
CVLT Trials 1-5									0.498	0.013				
CVLT Long-Free Recall									0.480	0.018				

Figure e1. Cortical regions of interest. Fig e1A: ACR (red), SLF (blue), bCC (green), CST (purple), PCR (yellow); Fig e1B: gCC (green), EC (purple), IC (blue), sCC (red), SS (yellow); Fig e1C: fMin (green), IFOF (blue), and fMaj (purple)

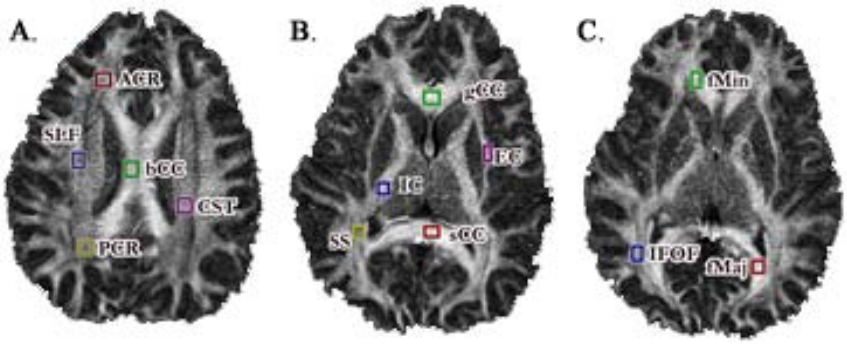

Figure e2. Methods for thalamic segmentation. Boundaries for identification of thalamic nuclei using the color-coded FA image, the T1-weighted SPGR, the primary eigenvector image, the T2-weighted FSE, and the black and white FA maps. 1B. Seed region placement and rules for placement for the anterior nucleus (AN, purple), ventral anterior nucleus (VA, red), dorsal-medial nucleus (DM, orange), ventral lateral nucleus (VL, blue), ventral posterior medial nucleus (VPM, yellow), pulvinar (PU, pink), and the ventral posterior lateral nucleus (VPL, green). 1C. Fiber tracts identified by these seed regions for a single subject.

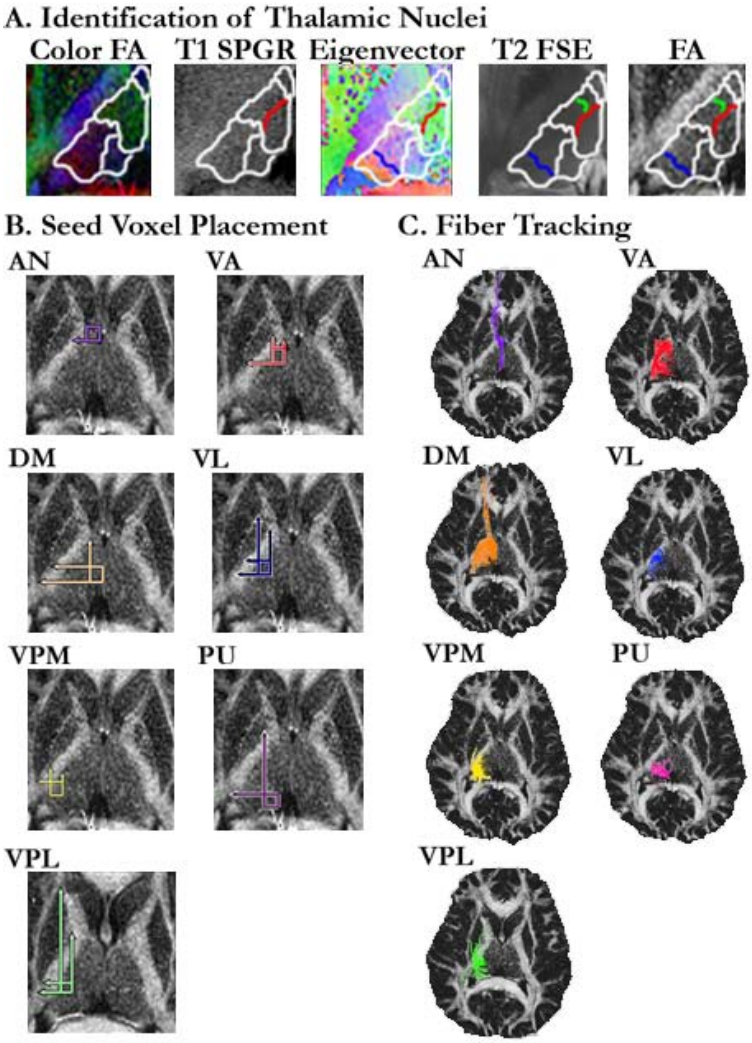

References Cited

1 Mori, S., Wakana, S., Nagae-Poetscher, L. & Van Zijl, P. *MRI Atlas of Human White Matter*. 1 edn, (Elsevier, 2005).

2 Wiegell, M. R., Tuch, D. S., Larsson, E. & Wedeen, V. J. Automatic segmentation of thalamic nuclei from diffusion tensor magnetic resonance imaging. *Neuroimage* **19**, 391-401 (2003).

3 Johansen-Berg, H. *et al.* Functional-anatomical validation and Individual variation of diffusion tractography-based segmentation of the human thalamus. *Cerebral Cortex* **15**, 31-39 (2005).

4 Magnotta, V., Gold, S., Andreasen, N., Ehrhardt, J. & Yuh, W. Visualization of sub-thalamic nuclei with cortex attenuated inversion recovery MR imaging. *Neuroimage* **11**, 341-346 (2000).

Appendix 2.

Little DM, Kraus MF, *Jiam C, *Moynihan M, *Siroko M, *Schulze E, *Geary EK. Imaging hypoxic-ischemic brain injury. *NeuroRehabilitation* (In Press).

Neuroimaging of Hypoxic-Ischemic Brain Injury

Deborah M. Little[1-4], Marilyn F. Kraus[1,5], Catherine Jiam[1], Michael Moynihan[1], Michelle Siroko[1,5], Evan Schulze[1], and Elizabeth K. Geary[1]

From the Departments of Neurology & Rehabilitation[1], Anatomy & Cell Biology[2], Ophthalmology & Visual Sciences[3], Psychology[4], and Psychiatry[5]

University of Illinois College of Medicine; Chicago Illinois 60612, USA

In Press, NeuroRehabilitation

Address for correspondence: Deborah M. Little PhD, Associate Professor of Neurology, University of Illinois College of Medicine, 912 South Wood Street 855N, Chicago, Illinois 60612, email: little@uic.edu or little.mri.lab@gmail.com, phone: 312.355.5405, fax: 312.355.5444.

Abstract

Hypoxic-ischemic brain injury (HI-BI) is a common cause of neurological morbidity in children and adults. Recent developments in neuroimaging techniques may permit *in vivo* identification of the structural and functional anatomy of HI-BI, and offer opportunities for the development of neuroimaging-guided prognosis. This article provides an update on the types and possible roles of currently-available neuroimaging techniques. The applications and limitations of these techniques to the study and clinical evaluation of persons with HI-BI are discussed, and the need of further research is highlighted.

Introduction

Hypoxic-ischemic brain injury is among the more common causes of mortality in developed countries, and most often affects pediatric and elderly populations. The effects of hypoxic-ischemic brain injury (HI-BI) on the brain are complex and involve a cascade of changes which can damage both neurons and white matter. The pathophysiology of HI-BI may involve injury to unmyelinated axons and neurons, including the oligodendrocytes which are responsible for myelination. HI-BI impacts neuronal structures through specific mechanisms such as glutamate excitotoxicity[29], release of inflammantory cytokines, iron accumulation [28], and an increase in free radicals [1]. In addition to directly damaging neuron cell bodies/dendrites, anoxia causes unmyelinated axonal depolarization leading to reversal of normal function in Na+- Ca^{2+} exchangers resulting in eventual exposure to toxic levels of Ca^{2+} [23]. Recent developments in neuroimaging have allowed better qualification and quantification of the effects of HI-BI *in vivo*. Although magnetic resonance imaging (MRI) is generally recognized to be the most sensitive imaging modality to the effects of HI-BI, computerized tomography (CT), positron emission tomography (PET), and single photon emission tomography (SPECT) still provide useful information in many circumstances. In some cases CT, PET, and SPECT are more sensitive to certain aspects of the neuropathology of HI-BI such as microbleeds and deficits in metabolic function. CT is the most prevalent imaging modality used throughout the world due to both its availability and relatively low cost. The recent introduction of multi-slice rapid CT scanners has increased its sensitivity to many of the effects of HI-BI on the brain, and has reinvigorated interest in the use of CT not only for clinical assessment but also in basic and applied clinical research. Similarly, there has been an increase in the use of and potential for PET to characterize the metabolic effects of HI-BI with the relatively recent advances and use of 2-[^{18}F] fluoro-2-deoxy-D-glucose (FDG) PET (FDG-PET). Electroencephalography (EEG) provides

additional clinical information by allowing a continuous monitoring of brain activity with high temporal resolution.

This article will review the use of each for clinical assessment and research applications in acute and chronic HI-BI at the level of the individual patient. Our assessment of validity and use of each method was driven by (1) ability to characterize and quantify the pathology common in different severities of HI-BI and (2) by correlation of these methods with functional outcome measures.

Computerized Tomography

At its most basic, computed tomography (CT) imaging involves the use of rotating x-ray equipment. Multiple x-rays are beamed into the body and the strength of these beams is measured as they leave the body. In dense tissue or bone, the residual x-ray beam is weaker, whereas in less dense tissue the residual x-ray is stronger. Information from the strengths of the transmitted beams is used to construct images of tissue density. CT imaging has the unique ability to offer clear images of different types of tissue, such as soft tissue, bone, muscle, and blood vessels. At present, the major neurologic clinical application of CT is in the acute assessment of blood and blood products. In addition to standard CT, CT perfusion allows quantification and assessment of cerebral perfusion which are especially important in HI-BI. Unlike standard CT, CT perfusion relies upon the repeated collection of a series of images to characterize the time-attenuation curves (TOC). In other words, CT perfusion is a change in CT intensity (or Hounsfield Unit, HU) over time following a bolus of iodine based contrast agent.

Although CT has proven useful in characterizing areas of ischemia in the brain as a result of overdose, carbon monoxide poisoning, and cardiac arrest in acute and subacute HI-BI, the conclusions that can be drawn from these studies are significantly limited by the extreme heterogeneity of patient age (in one study ages ranged from 2 months to 74 years and only included 10 patients) and mechanism of HI-BI (cardiac arrest, respiratory arrest, carbon monoxide, asphyxia, history of drug or alcohol abuse) as well as by lack of longitudinal studies correlating acute CT markers with long term outcome.

In general, acute insult to the brain that does not result in death is observed as areas of either increased (hyperintense) signal or decreased (hypointense) signal by CT. Although the effects of HI-BI are variable and locations of axonal injury diffusely distributed, gray matter structures such as the basal ganglia are the most common site of damage across patients with a history of cardiac arrest [47, 59] and carbon monoxide poisoning [37]. The hippocampus also may be differentially affected in HI-BI due to severe hypoglycemia [59]. Importantly, degree of damage to the basal ganglia (at least in patients with HI-BI secondary to cardiac arrest) also correlates with cognitive outcome [47]. In severe HI-BI due to cardiac or respiratory arrest common, acute CT findings include significant mass effects and midline shift [30]. In pediatrics, subarachnoid hemorrhage, diffuse axonal injury, increased intracranial pressure and disturbance of the blood brain barrier identified by CT in the acute stages are all associated with poor outcome [49].

Although there are a very limited number of studies validating CT findings with *ex vivo* examination, the few that have been conducted help define the limits of CT in acute characterization of the effects of HI-BI on structural integrity of the brain. Reports from the 1970s and 1980s indicate high concordance between CT and post-mortem examination in perinatal asphyxia (~90% concordance) [21] and weaker sensitivity of CT in adult ischemic injury (~65% concordance) with reduced concordance in small ischemic lesions [12]. However, there have not been large autopsy studies yet reported with newer multi-slice rapid CTs. The sensitivity of CT to small ischemic injury is likely much higher using newer methods.

In summary, although CT is superior for acute characterization of blood or mass effect in brain injury, the long term prognostic value is still unknown due to small sample sizes and heterogeneity.

Magnetic Resonance Imaging

Magnetic resonance-based imaging involves the interaction between a static magnetic field, local magnetic fields, and radio waves. While MRI is not the most used neuroimaging tool, it is the most

sensitive to the effects of HI-BI on neurons and white matter in the brain. MRI is exceptionally sensitive to hydrogen (in water) and to blood, but can be used to measure any atom which has an odd number of protons and is abundant in the human body. Such atoms include hydrogen, carbon-13, sodium, fluorine, and phosphorus. Conventional MR Imaging relies predominantly on hydrogen because of its abundance in the human body. However, sodium imaging has tremendous potential for evaluation of the effects of HI-BI on brain structure.

Generally, six main factors contribute to MRI. These include the properties of nuclear spin, the properties of the radio frequency (RF) excitation, properties of tissue relaxation, the strength of the static magnet field, the timing of RF pulses and the sensitivity of signal detection. The total MR signal is a combination of the sums of proton density reduced by T1, T2, and T2* relaxation. As such, each relaxation component offers distinct information about tissue character. T1-weighted images are generally more spatially sensitive making them useful in assessments of structure and volume. T2-weighted images are more sensitive to pathology, especially when that pathology affects local water content. Examples of the images generated by standard clinical MRI sequences at 3Tesla are presented in **Figure 1**.

Although conventional MRI sequences are able to identify contusions and lesions, these sequences are less sensitive to subtle axonal injury (e.g., diffuse axonal pathology resulting from traumatic brain injury (TBI)). It is likely for this reason that structural MRI measures are poor predictors of functional outcome [16] after TBI. Nonetheless, the strengths of standard structural measures of MRI, including accurate characterization and progression of atrophy (i.e., neuron loss) with high repeatability and without risk of multiple exposure to radiation, favor its use as a clinical and research tool for this and related purposes [46].

Characterization of HI-BI pathology generally relies upon T2-weighted fast spin echo imaging (T2FSE) which is excellent for significant white matter pathology; gradient echo imaging (GRE), which is the standard for characterization of blood product; and fluid attenuated imaging (FLAIR), which is sensitive to any change in local water density. In the case of more severe diffuse axonal injury secondary to HI-BI, FLAIR or fluid attenuated imaging has been used to characterize white matter lesions both in location and volume. Volume of hyperintense lesions on FLAIR in the acute stage have been associated with chronic changes in total gray and white matter cerebral volumes [19].

T2*-weighted gradient echo imaging is at present considered the most sensitive MRI marker of small hemorrhagic lesions and, in comparison to T2 FSE, was found to be more accurate at detecting lesions in the post-acute phase (~25 days post injury) in all cortical and brain stem regions.[24] But, when the predictive validity of both GRE and FSE were compared relative to outcome measures, both accounted for unique variance; this suggests that while GRE may be more sensitive to small hemorrhagic lesions, the concurrent use of T2 FSE provides additional information. Recent findings lead us to interpret this as indicating that T2 FSE has better sensitivity to diffuse axonal injury.

The usefulness of MRI for characterizing clinically-relevant HI-BI injury is in part dependent upon the age of the subject. Because of alterations in tissue contrast with normal development and myelination, the identification and differentiation of HI-BI-associated damage from normal development can be diagnostically challenging because both result in increased T2 signal. To assess the validity of MRI in this developing population, Liauw and colleagues [35] analyzed MR images for 75 patients under the age of 20 who showed increased T2 signal in the peritrigonal regions (the last to myelinate). Of the 75, 28 showed significant evidence of HI-BI. They found that the best MRI predictors of HI-BI (odds ratios from 14 to 25) were hyperintense signal on FLAIR (indicating increased local water content) and atrophy in the peritrigonal regions. Importantly, diffusion imaging (the most sensitive measure of traumatic brain injury) was not included in this analysis. When DWI is included in an imaging protocol in pediatric populations it has been found superior to all other modalities for detection of infarctions secondary to HI-BI[36]. Consistent with the traumatic brain injury literature, T2-weighted images are superior for identification of significant lesions [36] although still prove inferior to diffusion tensor imaging (DTI, discussed later in this article).

In adults, HI-BI due to cardiac arrest is associated with increased cortical (~25% of patients) and subcortical (~21% of patients) infarcts and atrophy in patients who survive the arrest [53]. In contrast, carbon monoxide poisoning in adults is associated with hyperintense lesions in the basal ganglia and diffusely in cerebral white matter [48, 66]. In patients with sustained cognitive and psychiatric symptoms at least 1 month post carbon monoxide poisoning, hyperintense lesions were found in the corpus callosum, subcortical projection fibers, and both internal and external capsules and hypointense lesions were found in basal ganglia. Lesions in the hippocampus are observed less frequently on MRI but have been reported [48].

Diffusion weighted imaging (DWI) provides assessment of the rate of water diffusion, which is the same along any direction. In adults with cardiac arrest leading to global cerebral anoxia, acute DWI showed abnormal basal ganglia, cerebellum and cortex. Subacutely, abnormalities were observed diffusely in cerebral gray and white matter. The DWI abnormalities were no longer present in chronic injury [2]. Lovblad and colleagues found similar results while studying 19 comatose patients between the ages of 2 days and 79 years with cortical ischemia [39]. DWI showed hyperintense signal and reduced ADC in cortical and basal ganglia regions. No abnormalities were identified on standard structural MRI. DWI also appears to be sensitive in acute severe trauma in predicting necrosis and outcome [42].

In summary, conventional structural MRI is an excellent tool for characterization of infarcts and lesions but less sensitive for characterization of more subtle axonal injury.

MR Perfusion-Weighted Imaging

Magnetic resonance-based perfusion-weighted (MRP) imaging provides measures of relative cerebral blood as well as characterization of regionally specific tissue transit times. MRP requires a series of lower spatial resolution images to be acquired covering the entire cerebral volume. These are acquired in concert with the injection of a bolus of intravenous contrast agent. This agent affects the local T2* signal. Over time, this increase signal can be followed to calculate the total time between injection and uptake in tissue. The total amount taken up into cerebral tissue is reflected in the calculation of relative cerebral blood volumes. Although the perfusion MRI is not commonly used in the assessment of neurotrauma or HI-BI, it is promising for this purpose and may be a useful tool for elucidating the imaging-neuropathological correlates of these conditions [13].

MRP may be especially valuable in severe hypoxic and/or ischemic damage. In patients with induced blood pressure elevation due to vasospasm there is a significant effect on total relative cerebral blood flow such that there is decreased tissue perfusion with increased (abnormal) blood pressure [26]. Additionally, MRP is highly sensitive to sustained cerebrovascular compromise that could induce additional tissue damage.

Additional evidence for the potential usefulness of MRP in HI-BI comes from an animal model of induced hypoxia-ischemia (HI) [18]. After 20 minutes of unilateral hypoxia, hypoperfusion was observed resulting in alterations in cerebral white matter. Even with reperfusion damage was observed in the hippocampus, cortex, and basal ganglia. In TBI patients significantly reduced rCBV was observed near contusions visualized with standard MRI. A subset of 4 patients also showed significant increases in rCBV around the contusion. The six patients with significantly altered rCBV around the contusion had worse clinical outcome [22]. Although at best preliminary, these findings, when taken together with the HI-BI animal findings and the ischemic stroke clinical literature, suggest that MRP may provide useful information regarding cerebral blood flow in the acute post-injury period (whether from HI-BI, TBI, or stroke) and that this information may guide interventions to reduce additional tissue compromise.

Although used routinely in clinical practice, MRP has not been applied or described in any large studies into the effects of HI-BI on cerebral perfusion abnormalities. This is one area of much needed research as it is well known that alterations in cerebral perfusion can affect development of atrophy and lesion size in stroke and as such, likely influence long term outcomes in HI-BI.

Functional Magnetic Resonance Imaging

Functional magnetic resonance imaging (fMRI), a derivative of MR imaging, allows for the visualization of task related brain activation [17]. During fMRI studies, a series of images (or volumes) are acquired as a participant performs a given task. The time-course of changes in local MR signal is then associated with the timing of the task being performed. To accomplish the temporal resolution required to investigate the time-course, spatial resolution is compromised. To overcome this significant limitation, the lower-resolution fMRI studies are generally statistically mapped onto a higher resolution anatomical scan.

fMRI uses the properties of blood flow and oxygen concentration changes that occur following neuronal firing to maps from which inferences about brain activation are drawn. Most fMRI studies utilize the blood oxygen level-dependent (BOLD) response for this purpose. This link between neural activation and CBF is the general basis of BOLD fMRI. When an area of the brain is activated by the demand to perform a task, the local neurons begin to fire and increase local metabolic activity. This increase in local metabolic activity leads to an increase in cerebral blood flow (CBF) to the activated area [52]. This is known as the hemodynamic response. This increase in CBF exceeds the demands of the activated neurons. The result is an increase in the concentration of local oxyhemoglobin associated with a relative decrease in deoxyhemoglobin. The paramagnetic properties of deoxyhemoglobin lead to a signal loss on T2* weighted sequences, that can be visualized as a transient increase in local signal in the capillary bed of activated neurons [38].

Although this technique offers substantial promise for the identification of the neural substrates of post-hypoxic neurological and neurobehavioral problems, fMRI has not been applied to the clinical or research evaluation of persons with HI-BI.

Magnetic Resonance Spectroscopy

Proton magnetic resonance spectroscopy (^{1}H MRS) utilizes the same physical equipment as standard MRI but allows the examination of neuronal intracellular metabolic status and provides information about neuronal integrity, hypoxia, inflammation, and axonal injury. The greatest limitation of MRS is that its value at low field strengths is limited because of the signal-to-noise ratio required to characterize the quantities of each chemical. Additionally, MRS is limited by the location of the brain area in question (poor quality near air and/or bone). MRS is a measure of resonance frequencies of different metabolites and chemicals. The small change in resonance frequency is known as the chemical shift. Common metabolites in MRS include myo-inositol (mI) a marker of the integrity of cell membranes, choline (Cho) which is associated with glial cell membrane integrity, creatine (Cr) a marker for ATP, glutamate (Glx), a marker of the neurotransmitter, N-acetyl aspartate (NAA) which is a marker for neuronal or dendrite integrity, lactate, which is a measure of hypoxia, and lipids which are an indicator of tissue necrosis. Generally speaking, decreases in the ratios NAA/Cr and NAA/Cho are markers of neuronal injury, while significant ischemic injury is associated with an increase in lactate and/or a decrease in NAA.

In neonatal MRS following HI-BI due to asphyxiation higher lactate and reduced N-acetylaspartate (NAA) is observed providing *in vivo* evidence of brain injury [5]. Importantly, both lactate and NAA correlated with neurologic and cognitive outcome [5]. In contrast, glutamate/creatine and glycine/creatine as well as the presence of a lactate peak correlated with outcome and injury severity in hypoxic ischemic encephalopathy in neonates [40]. Structural MRI identified lesions in the basal ganglia and hyperintensities and hemorrhage in periventricular regions but these did not prove as predictive of outcome as MRS measures. In near-drowning, pediatric patients with hyperintense basal ganglia lesions had the poorest functional outcome and had NAA/Creatine peaks. Additionally, NAA/Creatine correlated with hyperintense lesions in basal ganglia [20]. Similarly, reductions in NAA peak in near-drowning were consistently observed across 16 pediatric patients acutely following near-drowning and also correlated with outcome [33].

In summary, MRS has excellent potential for predictive validity in HI-BI and is sensitive to neuronal injury severity but again lacks validation. There is also a void of research in the value of this measure in adult patients. Finally, there is a lack of information available as to how medications commonly

used in intensive care settings affect MRS spectra. However, the reviewed results highlight the potential usefulness of MRS in HI-BI.

Diffusion Tensor Imaging

Diffusion tensor magnetic resonance imaging (DTI) is a relatively new technique that allows quantitative assessment of highly organized tissue, such as in white matter and nerve fibers. Myelin/white matter demonstrates relatively high resistance to ischemic damage due to fewer glutamate receptors [41]. However, the glial cells supporting myelination of axons, the oligodendrocytes, are vulnerable to ischemic effects of HI-BI. Damage to these cell and the resulting deleterious impact on myelinated axons can be observed using DTI. A unique application of DTI is to visualize the orientation and the connectivity of the white matter fiber tracts in the brain based on the principal diffusion directions [6-8]. This capability provides us with a new avenue to correlate the functional activation maps with structural changes in the fiber tracts (e.g., tract thickening, thinning, sprouting) throughout the course of neurological disorders. Importantly, DTI has shown sensitivity to alterations in the white matter microstructure independent of visible lesions [45].

DTI is a special form of diffusion-weighted imaging that allows the assessment and visualization of white matter and nerve fibers on a millimeter-level scale [10]. Although white and gray matter can be visualized and differentiated with standard MRI pulse sequences, standard MRI does not allow for the examination of the integrity or directionality of white matter tracts. DTI takes advantage of the diffusivity of water and the restrictions imposed on the diffusion of water by the myelin and axonal bodies associated with white matter fiber tracts. When fiber tracts are dense, for example, the restriction imposed by their density leads to directionally dependent or anisotropic diffusion. By analogy, if an ink drop is placed in a narrow or oval tube the diffusion of that ink drop will adjust to the shape of the tube. In contrast, if a drop of ink is placed in a large bowl of water the drop of ink will be more spherical or the diffusion will be fairly isotropic. It is this shape of the restriction of diffusion that is assessed with DTI. In well organized and intact white matter fiber tracts, the shape of water diffusion will occur preferentially along those tracts (i.e., more anisotropic). When there is less organization or a lack of aligned and organized fiber structures (i.e., gray matter, cerebrospinal fluid, axonal loss or demyelination) the shape of water diffusion will be more isotropic. Commonly, the degree of alignment and anisotropy is calculated as the fractional anisotropy (FA). FA values range from 0 to 1, where 0 represents isotropic diffusion and 1 represents anisotropic diffusion. Higher FA values are believed to represent such factors as degree of myelination and axonal density. The FA values are dependent not only upon the shape of diffusion (eigenvalues) but also the primary direction of diffusion (eigenvectors). These values can be combined in various methods to provide estimates of the axial and radial diffusivity in addition to more standard measures of water diffusion. Axonal diffusivity reflects the integrity of axonal bodies while radial diffusivity is a measure of the degree of myelination [31].

The power of DTI goes far beyond producing ADC, FA, RA, and other scalar-based maps. Although the specifics are still not well understood, FA is believed to reflect many factors including the degree of myelination and axonal density and/or integrity [3, 4, 25, 56, 57]. More discrete analysis of the axial ($\lambda_{\parallel}$) and radial diffusivity ($\lambda_{\perp}$) also provide potential measures of the mechanisms that underlie changes in white matter [50, 58]. $\lambda_{\parallel}$ reflects diffusivity parallel to axonal fibers. Increases in $\lambda_{\parallel}$ are thought to reflect pathology of the axon itself. $\lambda_{\perp}$ reflects diffusivity perpendicular to axonal fibers and appears to be more strongly correlated with myelin abnormalities, either dysmyelination or demyelination. DTI has also recently been used to characterize neuronal integrity in gray matter structures and may provide additional information about tissue integrity [63].

The last 5 years has seen a dramatic increase in the use of DTI to characterize the effects of trauma on brain structure as DTI does appear to be sensitive to diffuse axonal injury. Although very little has been completed on HI-BI, the TBI literature does offer some justification for the application of this methodology to the study of persons with HI-BI. In the late period following TBI, the most common finding is reduced FA that is proportional to the injury severity [44, 60, 67]. There is not yet a consensus as to what these changes mean in terms of neurobehavioral function. For example, in a

group of subjects with remote severe TBI and posttraumatic cognitive impairments there was no relationship between reduced FA in the corpus callosum and neuropsychological measures of memory or executive function, though there was a relationship with performance on the Mini-Mental State Examination [44]. However, Salmond and colleagues (in moderate to severe TBI) reported a relationship between reduced FA and measures of learning and memory [54]. Beyond cognition, FA apparently also accounts for significant variance in duration of post-traumatic amnesia [9].

Discrepancies in the relationships between cognition and FA are most likely due to differences in methodology including placement of regions of interest, variability in patient populations (including initial injury severity), and in the breadth of the neuropsychological testing. In work from our lab, FA from individual regions of interest showed some relationship with a variety of neuropsychological measures. However, the best correlate with cognitive function was a global measure of white matter integrity (the number of regions which showed reduced FA relative to controls) [32]. Similarly, others have reported modest correlations between measures of whole brain ADC and cognition.

The most promising DTI applications appear in the form of multimodal imaging studies. In at least one study using both magnetic resonance spectroscopy and DTI, outcome was more strongly predicted by the combination of FA and NAA/Cr ratios than either FA or NAA/Cr alone [61]. Another recent study combined DTI and magnetoencephalography (MEG) to characterize the relationship between integrity of white matter and the ability of MEG to assess neuronal activation with high temporal resolution. Although a very small sample size was used (n=10) the results are promising. In regions with reduced integrity of FA, there was also slowing of MEG waves suggesting that the lack of connectivity affected local neuronal function. Interestingly none of the 10 patients had lesions present on standard neuroimaging [27]. Studies utilizing multimodal MRI to include DTI and MR Spectroscopy, DTI and PET, or DTI and SPECT will likely prove immensely valuable for characterizing individual differences in recovery from or damage due to HI-BI and for characterizing the downstream effects of reductions in white matter tract integrity.

Neonates with hypoxic-ischemic encephalopathy who were scanned within the acute/sub-acute window showed significant FA reductions in the cerebral white matter, basal ganglia and thalamic injury. Apparent diffusion coefficient (ADC) was reduced only with more severe injury. Furthermore, ADC became less sensitive in the second and third week, whereas FA remained sensitive throughout.

Arterial Spin Labeling

Arterial Spin Labeling (ASL), an alternative to the BOLD method of neuroimaging, combines fMRI's ability to measure cerebral blood flow with the benefits of exogenous contrast agents, while remaining a noninvasive technique. ASL allows for the characterization of blood flow within brain tissue, but allows for direct visualization, rather than the indirect measure provided by the BOLD method. Perfusion is quantified by measuring the magnetic state of inflowing blood in relation to the magnetic state of static tissue. ASL is, in particularly relevant to the study of the acute and long term effects of HI-BI in the brain because it is potentially not affected by differential vasodilatation effects which can be complicated by acute medication usage.

ASL allows for rapid quantitative measurements of perfusion in the brain [64]. Much like PET, ASL takes advantage of the principles of exogenous tracers. Instead of invasive radiotracer injection, however, in ASL arterial blood water is first magnetized or 'labeled', then imaged via MRI. Arterial blood water is labeled immediately below the region of interest via a 180-degree radiofrequency inversion pulse. The application of this pulse to the region below the slice of interest results in inversion of the net magnetization of the blood water; that is, the water molecules in the blood are now magnetically labeled and can be detected via MR imaging. After a period of time known as the 'transit time,' the magnetically labeled (i.e. paramagnetic) blood water travels to the region of interest and exchanges with the un-magnetized water present in the tissue altering total tissue magnetization. During this inflow of the inverted spin water molecules, total tissue magnetization is reduced, thereby reducing the MR signal and image intensity. At this point, an image (known as the 'tag image') is taken. The experiment is then repeated without labeling the arterial blood to create another image (known as the 'control image'). To produce an image showing blood perfusion, the tag image is

subtracted from the control image. The resulting image reflects the total amount of arterial blood delivered to each voxel in the region of interest within the transit time [62].

Several methods of ASL perfusion imaging exist. In continuous ASL (CASL), a continuous radiofrequency pulse is applied to the targeted region below the slice of interest, resulting in continuous inversion of the magnetization of arterial blood water. Because of this continuous inversion, a steady-state develops in which regional magnetization in the brain is directly related to cerebral blood flow [11]. In pulsed ASL (PASL), a short (approximately 10 milliseconds) radiofrequency pulse is used to label blood water spins over a very specific area [62], which allows for minimization of the distance between the labeling region and the imaging slice [11]. Both have advantages and disadvantages.

At present, only a single report of the use of ASL in HI-BI is available to highlight the potential usefulness of this neuroimaging method in this population. In this study, 16 patients ranging in age from ~ 1-78 years of age following either anoxic or hypoxic-ischemic injury [51]. The imaging was conducted on after 5 days following the incident. Of the 16 patients, all but one showed significant hyperperfusion ipsilateral to the lesion and all but 4 did not survive to the 4 month follow-up. The authors interpreted these findings as suggestive of injury-induced loss of vascular autoregulation. Although this study does not provide evidence for the feasibility and use of ALS in milder forms of HI-BI or other neurotrauma, it does suggest that this technique may permit useful, and serial, visualization of cerebral perfusion that is without significant risk to patients. However, ASL is relatively new and because low signal-to-noise is better, it needs to be conducted at higher-field MRIs (3T and above) [65]. The requirement of relatively high-field MRIs for the performance of ASL will limit its widespread application for at least the next several years.

Support for the application of ASL to acute HI-BI comes from one study in pediatric ischemic stroke. Chen and colleagues reported perfusion abnormalities in 7 of the 10 children studied (5 hypoperfusion, 2 hyperpersion). The perfusion abnormalities were associated with stenosis, lesions, and final stroke volume [14]. Similarly, in adults, with symptomatic atherosclerotic disease regional cerebral blood flow (rCBF) calculated from ASL was associated with higher rCBF in a sample of 130 patients [64].

Positron Emission Tomography

PET imaging applications include functional neuroimaging, metabolic imaging, and evaluation of specific pathology using a given tracer. PET functional neuroimaging is based on an assumption that areas of high blood flow (due to neuronal activity) are also areas of high radioactivity. PET uses a tracer that releases positrons that annihilate with electrons and subsequently form a pair of gamma photons [15], which allows for excellent localization of the source of that radioemission. PET utilizing 2-[^{18}F]fluoro-2-deoxy-D-glucose, or FDG-PET, employs a glucose analog to monitor metabolic activity by highly metabolic organs and lesions [43]. The glucose analog is taken up by glucose utilizing cells, where it is phosphorylated and therefore “trapped” until it decays.

The application of PET to TBI is quite common. However, the application of PET to HI-BI is severely limited. In a small sample of 8 patients post-cardiac arrest HI-BI was associated with a decrease in cerebral glucose metabolism [55].

Conclusions

HI-BI produces neurological, cognitive, and other neurobehavioral impairments as well as substantial functional disability. The presence and severity of these impairments appears related to severity of injury as well as other pre- and post-injury variables (e.g., age at time of injury, cardiac arrest vs. other mechanism of injury, etc.). Recent developments in neuroimaging, especially with MRI, have added a variety of techniques that offer opportunities to improve the characterization of neural injury and to predict outcome. Unfortunately, the clinical and research application of these techniques to the study and treatment of persons with HI-BI remains very limited. Based on those data, and by analogy

from the study of other types of acquired brain injury [34], DTI and MRS are particularly promising with respect to their role in outcome prediction after HI-BI. Additionally, coupled structural and functional neuroimaging techniques, whether MRI-PET or various combinations of structural and functional MRI , are needed to identify the mechanisms that better explain the neurological and neurobehavioral impairments and that predict functional outcomes after HI-BI.

Acknowledgements

The authors gratefully acknowledge the support of grants from the Department of Defense and Congressional Directed Medical Research Program Grant PT075675 (DML), National Institute on Aging Grant AG028662 (DML), National Institute of Mental Health Grant MH068787 (MFK) and the Marshall Goldberg TBI Research Fund (MFK). The contents of this paper are solely the responsibility of the authors and do not necessarily represent the official views of the University of Illinois at Chicago, the Department of Defense or the National Institutes of Health.

Figure Captions and Figures

Figure 1. Standard clinical MRI protocols used in the evaluation of persons with HI-BI performed at 3Tesla. (A) T1-weighted spoiled gradient volume (SPGR); (B) T2-weighted fluid attenuated sequence (FLAIR); (C) T2-weighted fast spin echo (FSE); (D) gradient echo (GRE); (E) fractional anisotropy (FA) calculated from DTI ; and (E) apparent diffusion coefficient (ADC) maps also calculated from DTI.

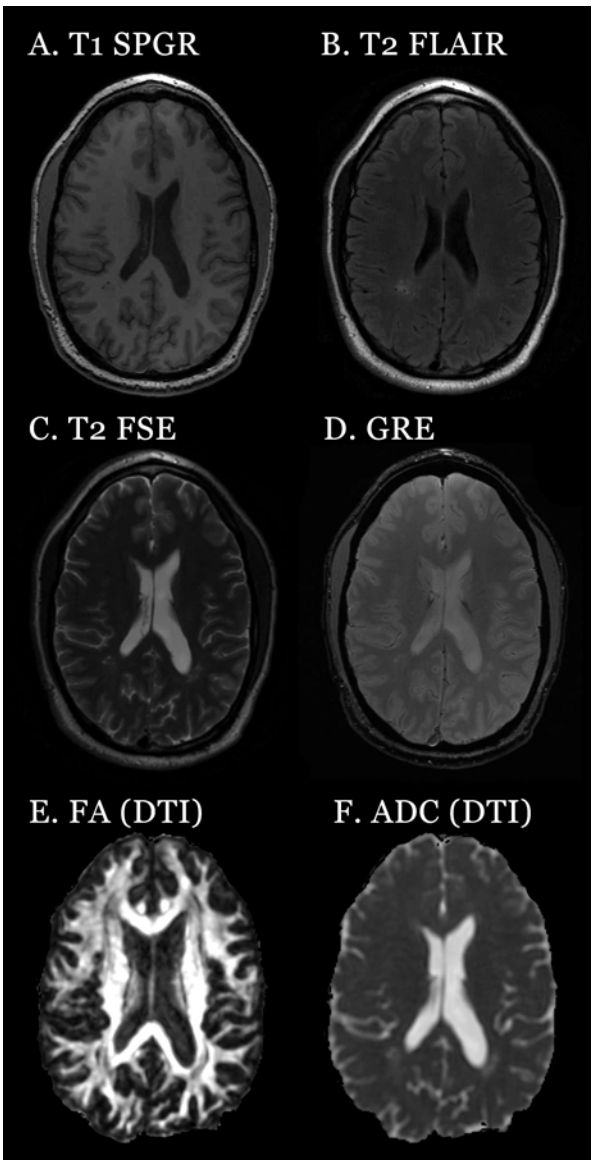

References

[1] M. Amato, F. Donati, Update on perinatal hypoxic insult: mechanism, diagnosis and interventions, Eur J Paediatr Neurol 4 (2000) 203-209.

[2] A. Arbelaez, M. Castillo, S.K. Mukherji, Diffusion-weighted MR imaging of global cerebral anoxia, American Journal Of Neuroradiology 20 (1999) 999-1007.

[3] K. Arfanakis, D. Cordes, V.M. Haughton, J.D. Carew, M.E. Meyerand, Independent component analysis applied to diffusion tensor MRI, Magnetic Resonance in Medicine 47 (2002) 354-363.

[4] K. Arfanakis, V.M. Haughton, J.D. Carew, B.P. Rogers, R.J. Dempsey, M.E. Meyerand, Diffusion tensor MR imaging in diffuse axonal injury, American Journal of Neuroradiology 23 (2002) 794-802.

[5] A.J. Barkovich, K. Baranski, D. Vigneron, J.C. Partridge, D.K. Hallam, B.L. Hajnal, D.M. Ferriero, Proton MR spectroscopy for time evaluation of brain injury in asphyxiated, term neonates, American Journal Of Neuroradiology 20 (1999) 1399-1405.

[6] P. Basser, J. Mattiello, D. Lebihan, MR diffusion tenser spectroscopy and imaging, 66 (1994) 259-267.

[7] P. Basser, S. Pajevic, C. Pierpaoli, J. Duda, A. Aldroubi, In vivo fiber tractography using DT-MRI data, Magnetic Resonance in Medicine 44 (2000) 625-632.

[8] P. Basser, C. Pierpaoli, Microstructural and physiological features of tissues elucidated by quantitative-diffusion-tensor MRI, J of Magnetic Resonance 111 (1996) 209-219.

[9] R.R. Benson, S.A. Meda, S. Vasudevan, Z.F. Kou, K.A. Govindarajan, R.A. Hanks, S.R. Millis, M. Makki, Z. Latif, W. Coplin, J. Meythaler, E.M. Haacke, Global white matter analysis of diffusion tensor images is predictive of injury severity in traumatic brain injury, Journal Of Neurotrauma 24 (2007) 446-459.

[10] D. Bihan, J. Mangin, P. C, e. al., Diffusion tensor imaging: concepts and applications., J. Magn Reson Imaging 13 (2001) 534-543.

[11] F. Calamante, D.L. Thomas, G.S. Pell, J. Wiersma, R. Turner, Measuring cerebral blood flow using magnetic resonance imaging techniques, Cerebral Blood Flow & Metabolism 19 (1999) 701-735.

[12] J. Campbell, O. Houser, J. Stevens, e. al, Computed tomography and radionuclide imaging in the evaluation of ischemic stroke., Radiology 126 (1978) 695-708.

[13] I. Cernak, Z. Wang, J. Jiang, X. Bian, J. Savic, Ultrastructural and functional characteristics of blast injury-induced neurotrauma, Journal of Trauma-Injury Infection & Critical Care 50 (2001) 695-706.

[14] Z. Chen, P. Ni, J. Zhang, Y. Ye, H. Xiao, G. Qian, S. Xu, J. Wang, X. Yang, J. Chen, B. Zhang, Y. Zeng, Evaluating ischemic stroke with diffusion tensor imaging, Neurological Research 30 (2008) 720-726.

[15] C.P. Derdeyn, Positron Emission Tomography Imaging of Cerebral Ischemia, PET Clin 2 (2007) 35-44.

[16] P. Diaz-Marchan, L. Hayman, D. Carrier, D. Feldman, Computed tomography of closed head injury. In: R. Narayan, J. Wilburger, J. Povlishock (Eds.), Neurotrauma, McGraw-Hill, New York, 1996.

[17] B.C. Dickerson, Advances in Functional Magnetic Resonance Imaging: Technology and Clinical Applications, Neurotherapeutics: The Journal of the American Society for Experimental NeuroTherapeutics 4 (2007) 360-370.

[18] R.M. Dijkhuizen, S. Knollema, H.B. van der Worp, G.J. Ter Horst, D.J. De Wildt, J.W.B. van der Sprenkel, K.A.F. Tulleken, K. Nicolay, Dynamics of cerebral tissue injury and perfusion after temporary hypoxia-ischemia in the rat - Evidence for region-specific sensitivity and delayed damage, Stroke 29 (1998) 695-704.

[19] K. Ding, C.M. de la Plata, J.Y. Wang, M. Mumphrey, C. Moore, C. Harper, C.J. Madden, R. McColl, A. Whittemore, M.D. Devous, R. Diaz-Arrastia, Cerebral Atrophy after Traumatic White Matter Injury: Correlation with Acute Neuroimaging and Outcome, Journal Of Neurotrauma 25 (2008) 1433-1440.

[20] D.J. Dubowitz, S. Bluml, E. Arcinue, R.B. Dietrich, MR of hypoxic encephalopathy in children after near drowning: Correlation with quantitative proton MR spectroscopy and clinical outcome, American Journal Of Neuroradiology 19 (1998) 1617-1627.

[21] O. Flodmark, L. Becker, M. Harwood-Nash, P. Fitzhardinge, C. Fitz, S. Chuang, Correlation between computed tomography and autopsy in premature and full-term neonates that have suffered perinatal asphyxia., Neuroradiology 137 (1980) 93-103.

[22] M.R. Garnett, A.M. Blamire, R.G. Corkill, B. Rajagopalan, J.D. Young, T.A.D. Cadoux-Hudson, P. Styles, Abnormal cerebral blood volume in regions of contused and normal appearing brain following traumatic brain injury using perfusion magnetic resonance imaging, Journal Of Neurotrauma 18 (2001) 585-593.

[23] G. Garthwaite, G. Brown, A. Batchelor, D. Goodwin, J. Garthwaite, Mechanisms of ischaemic damage to central white matter axons: a quantitative histological analysis using rat optic nerve, Neuroscience 94 (1999) 1219-1230.

[24] D.J. Gerber, A.H. Weintraub, C.P. Cusick, P.E. Ricci, G.G. Whiteneck, Magnetic resonance imaging of traumatic brain injury: relationship of T2 SE and T2*GE to clinical severity and outcome, Brain Injury 18 (2004) 1083-1097.

[25] L. Harsan, P. Poulet, B. Guignard, J. Steibel, N. Parizel, P. de Sousa, N. Boehm, D. Grucker, M. Ghandour, Brain dysmyelination and recovery assessment by noninvasive in vivo diffusion tensor magnetic resonance imaging., J Neurosci Res 83 (2006) 392-402.

[26] A. Hillis, J. Ilatowski, P. Barker, M. Torbey, W. Ziai, N. Beauchamp, S.H. Oh, R. Wityk, A pilot randomized trial of induced blood pressure elevation: effects on functional and focal perfusion in acute and subacute stroke., Cerebrovasc Dis 16 (2003) 236-246.

[27] M. Huang, R.J. Theilmann, A. Robb, A. Angeles, S. Nichols, A. Drake, J. Dandrea, M. Levy, M. Holland, T. Song, S. Ge, E. Hwang, K. Yoo, L. Cui, D.G. Baker, D. Trauner, R. Coimbra, R.R. Lee, Integrated imaging approach with MEG and DTI to Detect Mild Traumatic Brain Injury in Military and Civilian Patients, Journal of Neurotrauma (2008).

[28] C. Kaur, E. Ling, Increased expression of transferrin receptors and iron in amoeboid microglial cells in postnatal rats following an exposure to hypoxia, Neurosci Lett 262 (1999) 183-186.

[29] C. Kaur, V. Sivakumar, L. Ang, A. Sundaresan, Hypoxic damage to the periventricular white matter in neonatal brain: role of vascular endothelial growth factor, nitric oxide and excitotoxicity, J Neurochem 98 (2006) 1200-1216.

[30] B. Kjos, M. Brantzawadzki, R. Young, Early CT findings of global central nervous-system hypoperfusion, American Journal Of Roentgenology 141 (1983) 1227-1232.

[31] M. Kraus, T. Susmaras, B. Caughlin, C. Walker, J. Sweeney, D. Little, White matter integrity and cognition in chronic traumatic brain injury: a diffusion tensor imaging study., Brain 130 (2007) 2508-2519.

[32] M.F. Kraus, T. Susmaras, B.P. Caughlin, C.J. Walker, J.A. Sweeney, D.M. Little, White matter integrity and cognition in chronic traumatic brain injury: a diffusion tensor imaging study, Brain 130 (2007) 2508-2519.

[33] R. Kreis, E. Arcinue, T. Ernst, T.K. Shonk, R. Flores, B.D. Ross, Hypoxic encephalopathy after near-drowning studied by quantitative H-1-magnetic resonance spectroscopy - Metabolic changes and their prognostic value, Journal Of Clinical Investigation 97 (1996) 1142-1154.

[34] B. Levine, N. Kovacevic, E.I. Nica, G. Cheung, F. Gao, M.L. Schwartz, S.E. Black, The Toronto traumatic brain injury study: injury severity and quantified MRI, Neurology 70 (2008) 771-778.

[35] L. Liauw, J. van der Grond, V. Slooff, F.W.D. Bruine, L. Laan, S. le Cessie, M. van Buchem, G. van Wezel-Meijler, Differentiation between peritrigonal terminal zones and hypoxic-ischemic white matter injury on MRI, European Journal Of Radiology 65 (2008) 395-401.

[36] L. Liauw, J. Van der Grond, A.A. Van den Berg-Huysmans, I.H. Palm-Meinders, M.A. Van Buchem, G. Van Wezel-Meijler, Hypoxic-ischemic encephalopathy: Diagnostic value of conventional MR imaging pulse sequences in term-born neonates, Radiology 247 (2008) 204-212.

[37] C.P. Lo, S.Y. Chen, K.W. Lee, W.L. Chen, C.Y. Chen, C.J. Hsueh, G.S. Huang, Brain injury after acute carbon monoxide poisoning: Early and late complications, American Journal Of Roentgenology 189 (2007) W205-W211.

[38] N.K. Logothetis, B.A. Wandell, Interpreting The BOLD Signal, Annual Review of Physiology 66 (2004) 735-769.

[39] K.O. Lovblad, S.G. Wetzel, T. Somon, K. Wilhelm, A. Mehdizade, A. Kelekis, M. El-Koussy, S. El-Tatawy, M. Bishof, G. Schroth, S. Perrig, F. Lazeyras, R. Sztajzel, F. Terrier, D. Rufenacht, J. Delavelle, Diffusion-weighted MRI in cortical ischaemia, Neuroradiology 46 (2004) 175-182.

[40] G.K. Malik, M. Pandey, R. Kumar, S. Chawla, B. Rathi, R.K. Gupta, MR imaging and in vivo proton spectroscopy of the brain in neonates with hypoxic ischemic encephalopathy, European Journal Of Radiology 43 (2002) 6-13.

[41] F. Marcoux, R. Morawetz, R. Crowell, U. DeGirolami, J. Haksey, Differential regional vulnerability in transient focal cerebral ischemia, Stroke 13 (1982) 339-346.

[42] A.M. McKinney, M. Teksam, R. Felice, S.O. Casey, R. Cranford, C.L. Truwit, S. Kieffer, Diffusion-weighted imaging in the setting of diffuse cortical laminar necrosis and hypoxic-ischemic encephalopathy, American Journal Of Neuroradiology 25 (2004) 1659-1665.

[43] R.S. Miletich, Positron Emission Tomography for Neurologists, Neurol Clin 27 (2008) 61-88.

[44] N. Nakayama, A. Okamura, e. al., Evidence for white matter disruption in traumatic brain injury without macroscopic lesions., J Neurol Neurosurg Psychiatry 77 (2006) 850-855.

[45] N. Nakayama, A. Okumura, J. Shinoda, Y.-T. Yasokawa, K. Miwa, S.-I. Yoshimura, T. Iwama, Evidence for white matter disruption in traumatic brain injury without macroscopic lesions., J Neurol Neurosurg Psychiatry 77 (2006) 850-855.

[46] K. Ng, D.J. Mikulis, J. Glazer, N. Kabani, C. Till, G. Greenberg, A. Thompson, D. Lazinski, R. Agid, B. Colella, R.E. Green, Magnetic resonance imaging evidence of progression of subacute brain atrophy in moderate to severe traumatic brain injury, Archives of Physical Medicine & Rehabilitation 89 (2008) S35-44.

[47] B. Nunes, J. Pais, R. Garcia, Z. Magalhaes, C. Granja, M.C. Silva, Cardiac arrest: long-term cognitive and imaging analysis, Resuscitation 57 (2003) 287-297.

[48] P. O'Donnell, P.J. Buxton, A. Pitkin, L.J. Jarvis, The magnetic resonance imaging appearances of the brain in acute carbon monoxide poisoning, Clinical Radiology 55 (2000) 273-280.

[49] L.-C. Ong, B. Selladurai, M. Dhillon, M. Atan, M.-S. Lye, The Prognostic Value of the Glasgow Coma Scale, Hypoxia and Computerised Tomography in Outcome Prediction of Pediatric Head Injury, Pediatr Neurosurg 24 (1996) 285-291.

[50] C. Pierpaoli, A. Barnett, S. Pajevic, R. Chen, L. Penix, A. Virta, P. Basser, Water diffusion changes in wallerian degeneration and their dependence on white matter architecture, NeuroImage 13 (2001) 1174-1185.
[51] J.M. Pollock, C.T. Whitlow, A.R. Deibler, H. Tan, J.H. Burdette, R.A. Kraft, J.A. Maldjian, Anoxic injury-associated cerebral hyperperfusion identified with arterial spin-labeled MR imaging, American Journal Of Neuroradiology 29 (2008) 1302-1307.
[52] D. Purves, G.J. Augustine, D. Fitzpatrick, W.C. Hall, A.-S. LaMantia, J.O. McNamara, L.E. White (Eds.), Neuroscience, Sinauer Associates, Sunderland, 2008.
[53] R.O. Roine, R. Raininko, T. Erkinjuntti, A. Ylikoski, M. Kaste, Magnetic-Resonance-Imaging Findings Associated With Cardiac-Arrest, Stroke 24 (1993) 1005-1014.
[54] C. Salmond, D. Menon, D. Chatfield, G. Williams, A. Pena, B. Sahakian, J. Pickard, Diffusion tensor imaging in chronic head injury survivors: Correlations with learning and memory indices, Neuroimage 29 (2006) 117-124.
[55] A. Schaafsma, B.M. de Jong, J.L. Bams, H. Haaxma-Reiche, J. Pruim, J.G. Zijlstra, Cerebral perfusion and metabolism in resuscitated patients with severe post-hypoxic encephalopathy, Journal Of The Neurological Sciences 210 (2003) 23-30.
[56] S.-K. Song, S.-W. Sun, M. Ramsbottom, C. Chang, J. Russell, A. Cross, Dysmyelination revealed through MRI as increased radial (but unchanged axial) diffusion of water, NeuroImage 17 (2002) 1429-1436.
[57] S. Song, S. Sun, W. Ju, S. Lin, A. Cross, A. Neufeld, Diffusion tensor imaging detects and differentiates axon and myelin degeneration in mouse optic nerve after retinal ischemia, Neuroimage 20 (2003) 1714-1722.
[58] S. Song, S. Sun, M. Ramsbottom, C. Chang, J. Russell, A. Cross, Dysmyelination revealed through MRI as increased radial (but unchanged axial) diffusion of water., Neuroimage 17 (2002) 1429-1436.
[59] S. Takahashi, S. Higano, K. Ishii, K. Matsumoto, K. Sakamoto, Y. Iwasaki, M. Suzuki, Hypoxic Brain-Damage - Cortical Laminar Necrosis And Delayed Changes In White-Matter At Sequential Mr-Imaging, Radiology 189 (1993) 449-456.
[60] D. Tisserand, G. Staanisz, N. Lobaugh, E. Gibson, T. Li, S. Black, Diffusion tensor imaging for the evaluation of white matter pathology in traumatic brian injury., Brain And Cognition 60 (2006) 216-217.
[61] E. Tollard, D. Galanaud, V. Perlbarg, P. Sanchez-Pena, Y. Le Fur, L. Abdennour, P. Cozzone, S. Lehericy, J. Chiras, L. Puybasset, Experience of diffusion tensor imaging and 1H spectroscopy for outcome prediction in severe traumatic brain injury: Preliminary results., Critical Care Medicine 37 (2009) 1448-1455.
[62] University of Michigan Functional MRI Laboratory, Arterial Spin Labeling, (2007).
[63] D. Vaillancourt, M. Spraker, J. Prodoehl, I. Abraham, D. Corcos, X. Zhou, C. Comella, D. Little, High-resolution diffusion tensor imaging in the substantia nigra of de novo Parkinson disease, Neurology 72 (2009) 1378-1384.
[64] P.J. van Laar, Y. van der Graaf, W.P.T.M. Mali, J. van der Grond, J. Hendrikse, Effect of cerebrovascular risk factors on regional cerebral blood flow, Radiology 246 (2008) 196-204.
[65] J. Wang, D.J. Licht, Pediatric perfusion MR imaging using arterial spin labeling, Neuroimaging Clinics Of North America 16 (2006) 149-+.
[66] E.F.M. Wijdicks, N.G. Campeau, G.M. Miller, MR imaging in comatose survivors of cardiac resuscitation, American Journal Of Neuroradiology 22 (2001) 1561-1565.
[67] J. Xu, I.-A. Rasmussen, J. Lagopoulos, A. Haberg, Diffuse axonal injury in severe traumatic brain injury visualized using high-resolution diffusion tensor imaging, Journal of Neurotrauma 24 (2007) 753-765.